Supplement of Earth Syst. Sci. Data, 17, 7035–7054, 2025
https://doi.org/10.5194/essd-17-7035-2025-supplement

Supplement of

Global biogenic isoprene emissions 2013–2020 inferred from satellite isoprene observations

Hui Li et al.

Correspondence to: Hui Li (hui.li@lsce.ipsl.fr)

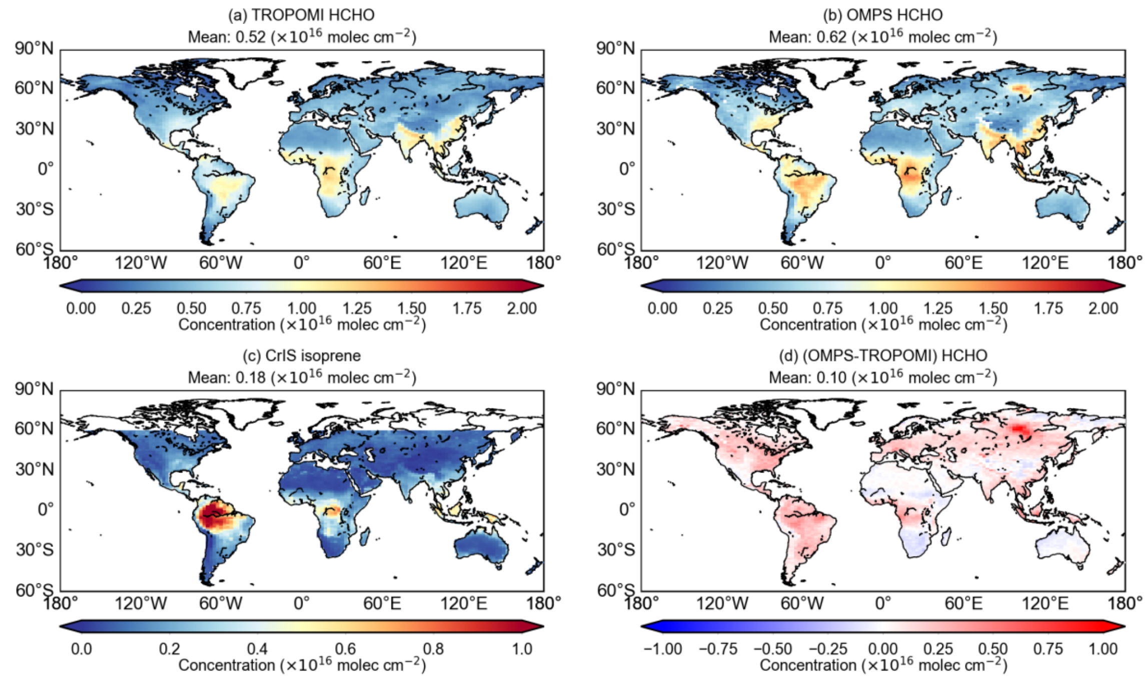

Figure S1. Global distribution of annual average HCHO and isoprene concentration in 2019. (a) and (b) present the HCHO concentration from TROPOMI and OMPS. (c) shows the isoprene concentration from CrIS. (d) shows the difference between OMPS and TROPOMI HCHO concentration.

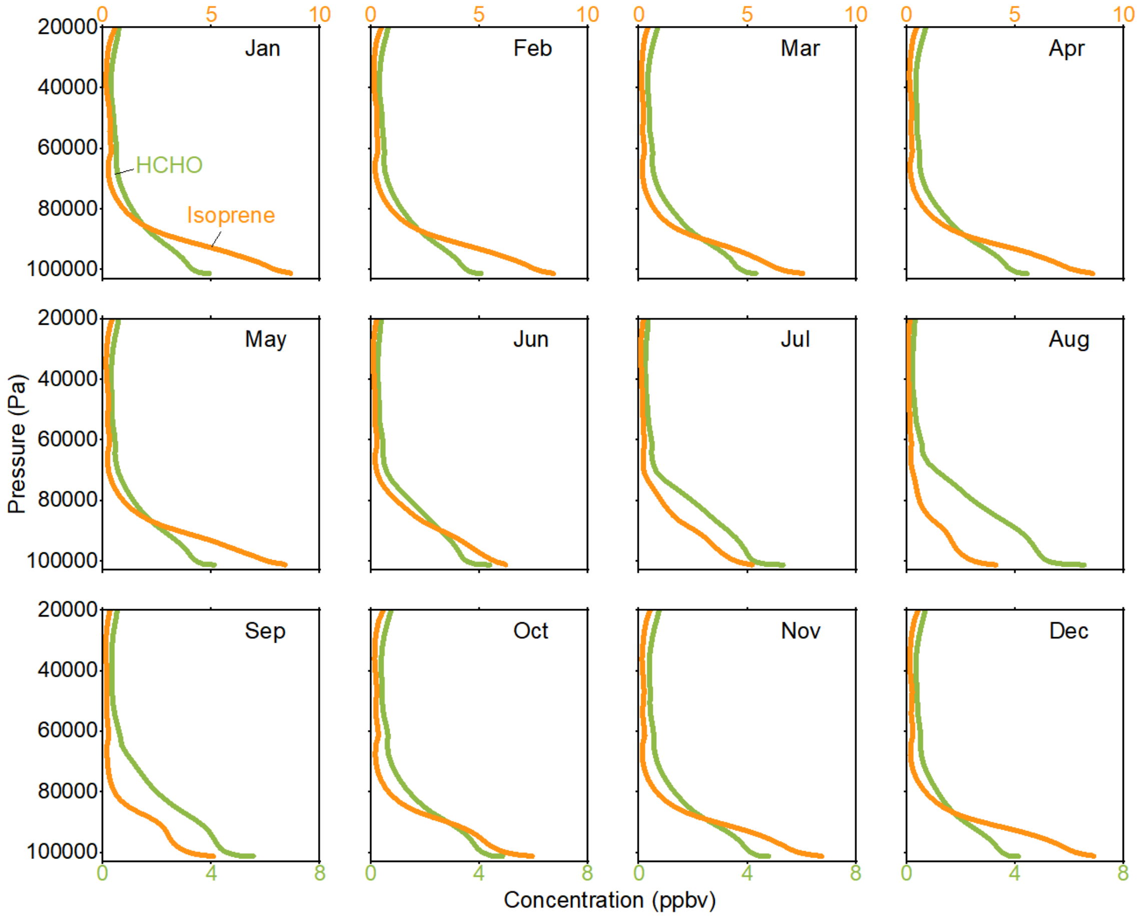

Figure S2. Vertical profile of LMDZ-INCA simulated isoprene (top x-axis) and HCHO (bottom x-axis) mixing ratios over Amazon region in each month in 2019.

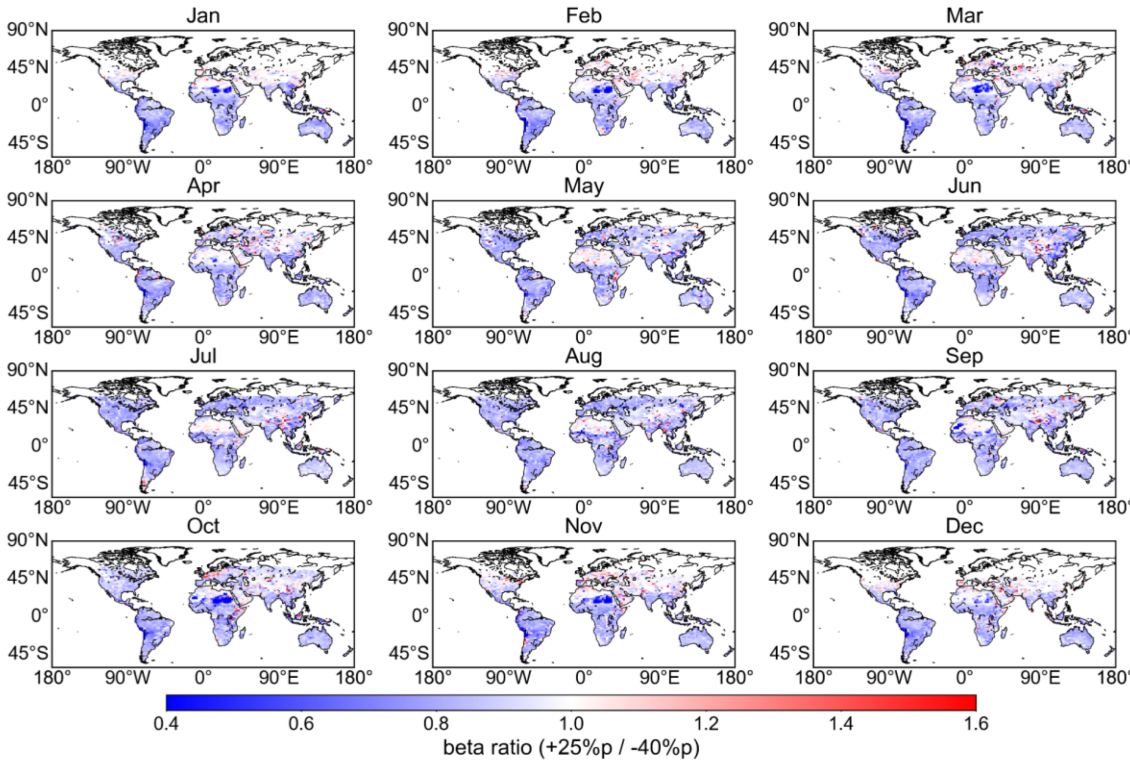

Figure S3. Distribution of ($\beta_{+25\%}/\beta_{-40\%}$) ratio in 2019.

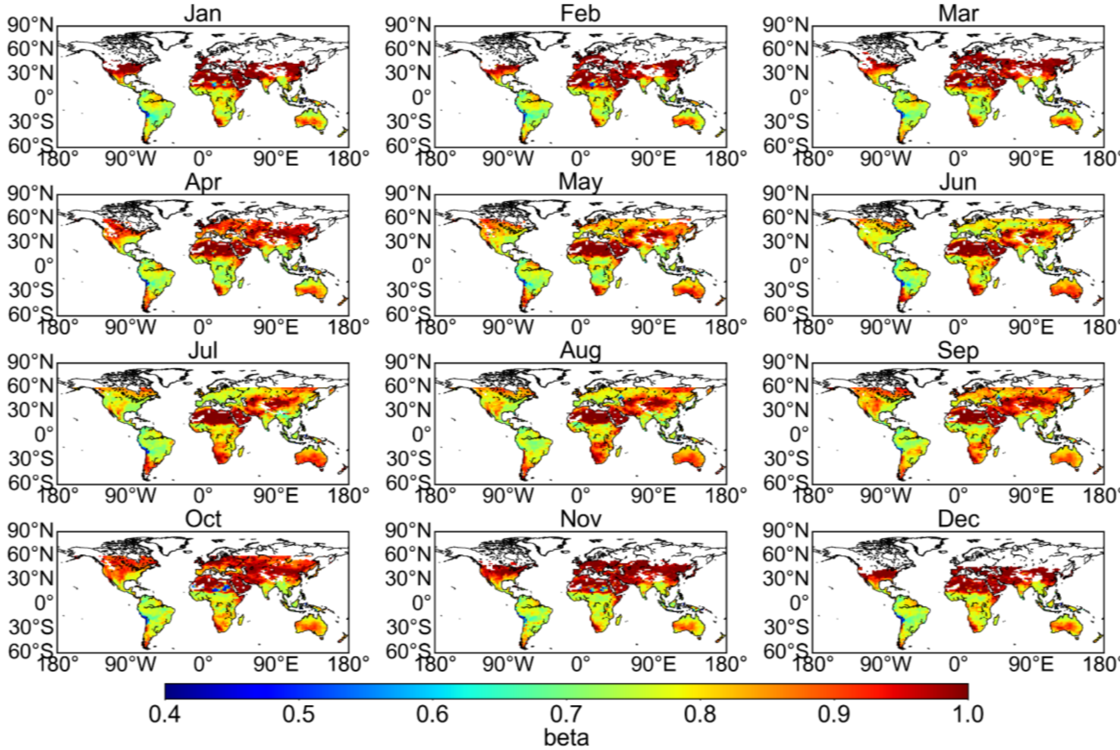

Figure S4. An example of monthly β distribution in 2019.

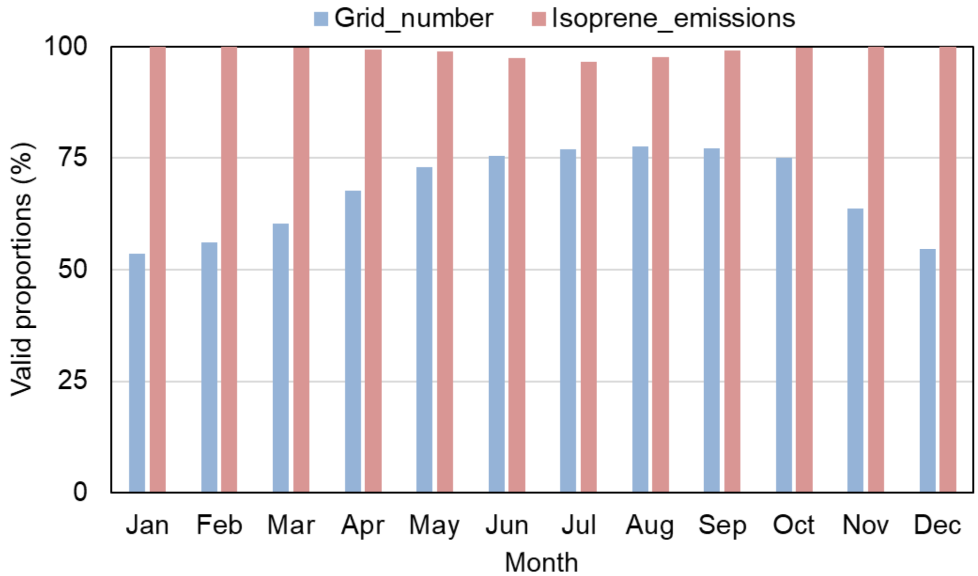

Figure S5. Proportions of grids with updated emissions, including the grid number proportions and emission proportions. We here use prior maps to calculate the proportions.

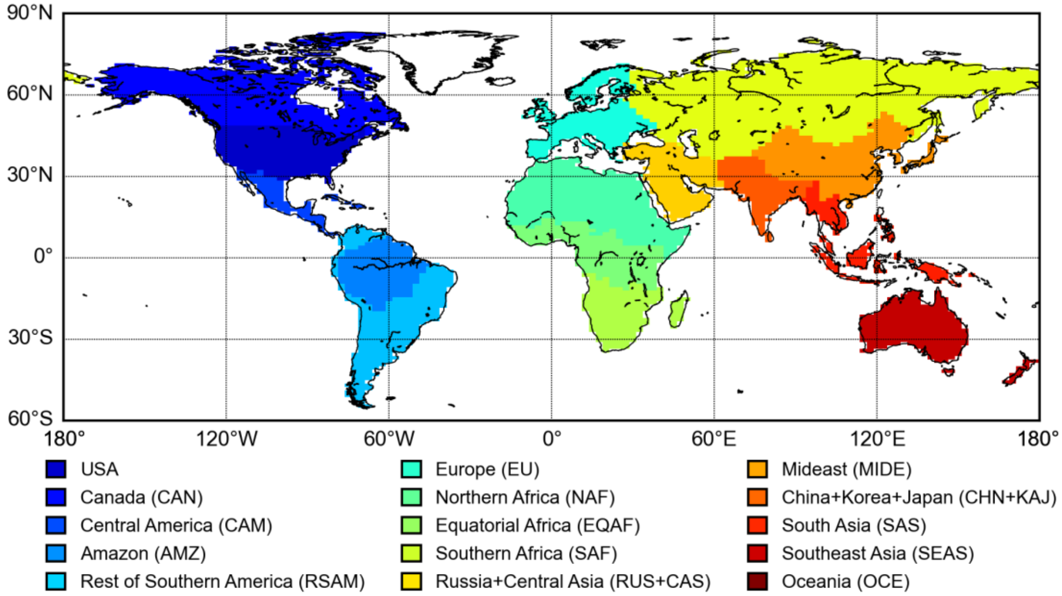

Figure S6. The 15-region classification in this study.

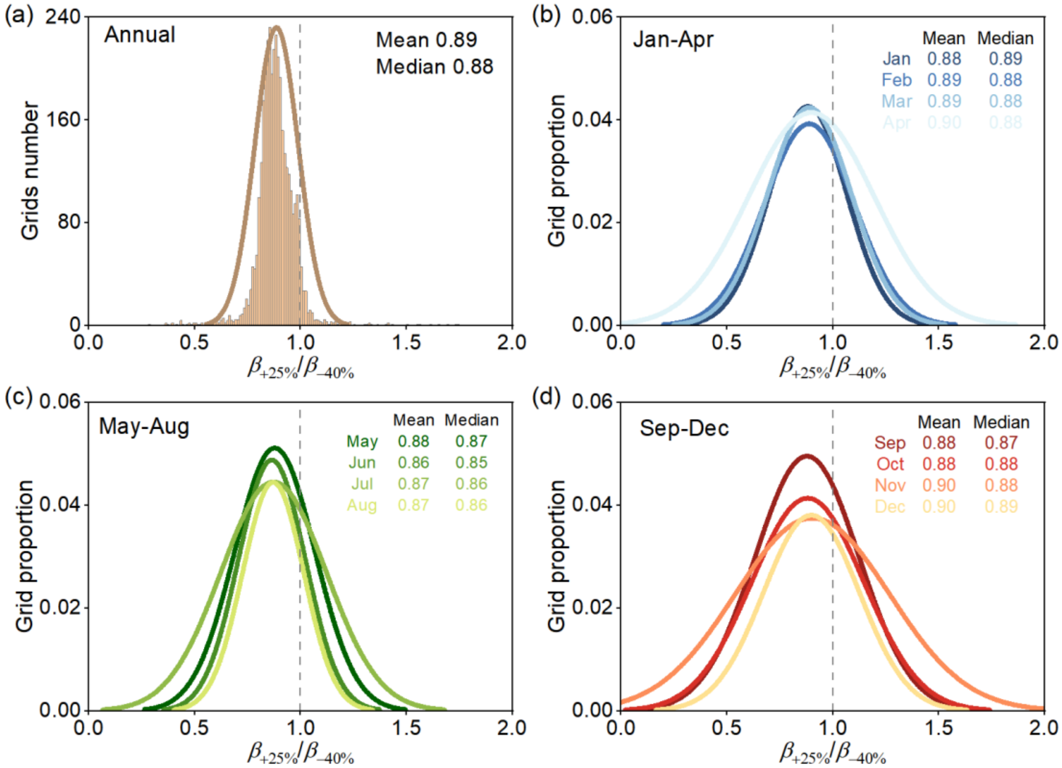

Figure S7. Statistical summary of the grid-scale β ratio ($\beta_{+25\%}/\beta_{-40\%}$) derived from the regression-based inversion in 2019. (a) shows the annual mean statistics, while (b)–(d) present the monthly distributions for Jan–Apr, May–Aug, and Sep–Dec, respectively. The tables inside (b)-(d) correspond to mean and median value of $\beta_{+25\%}/\beta_{-40\%}$ for each month.

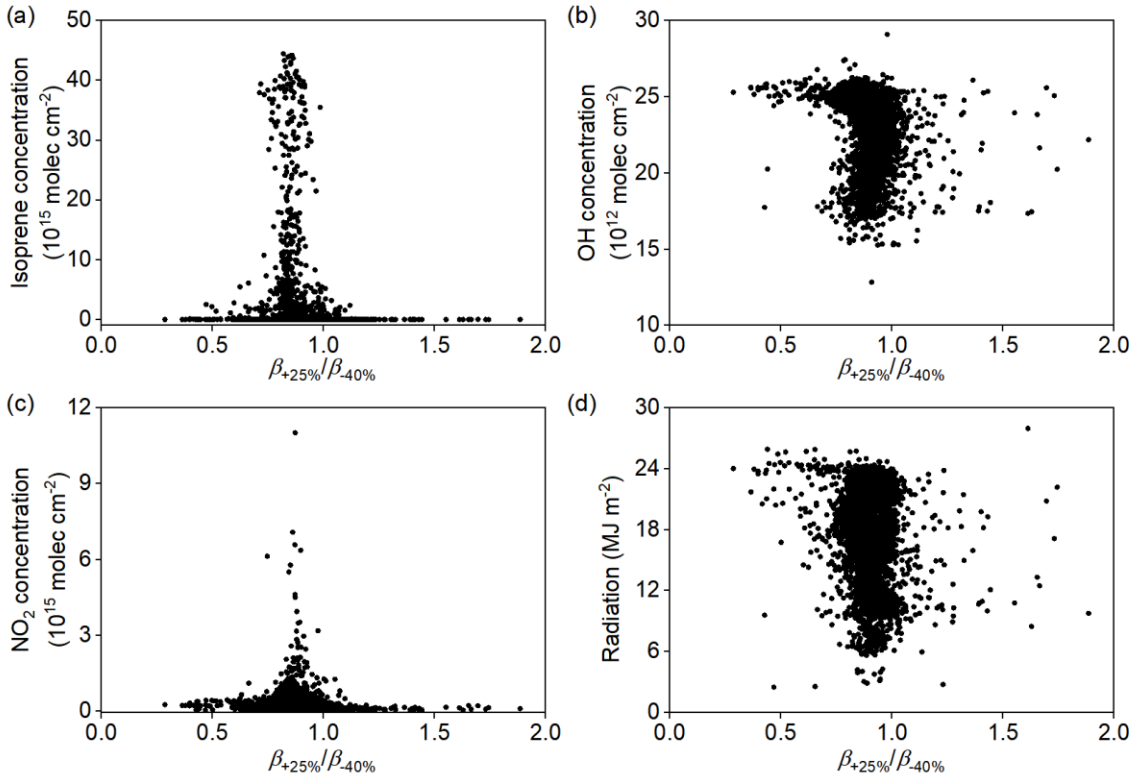

Figure S8. Correlation between annual mean grid-scale β ratio ($\beta_{+25\%}/\beta_{-40\%}$) and (a) simulated isoprene column concentrations, (b) simulated OH column concentrations, (c) simulated NO_2 column concentrations, and (d) radiation from ERA5.

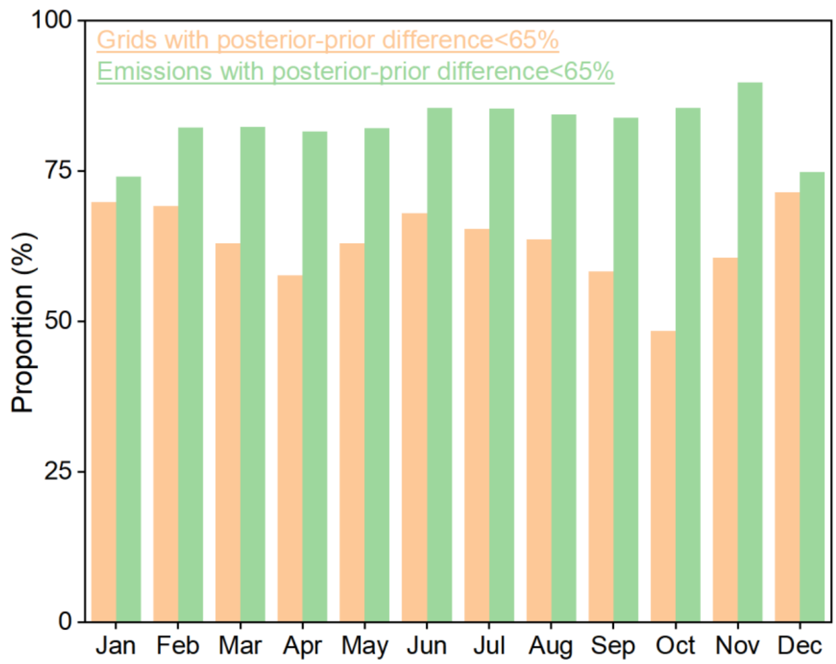

Figure S9. Statistics of grid number and their emission proportions of posterior-prior difference within ±65%.

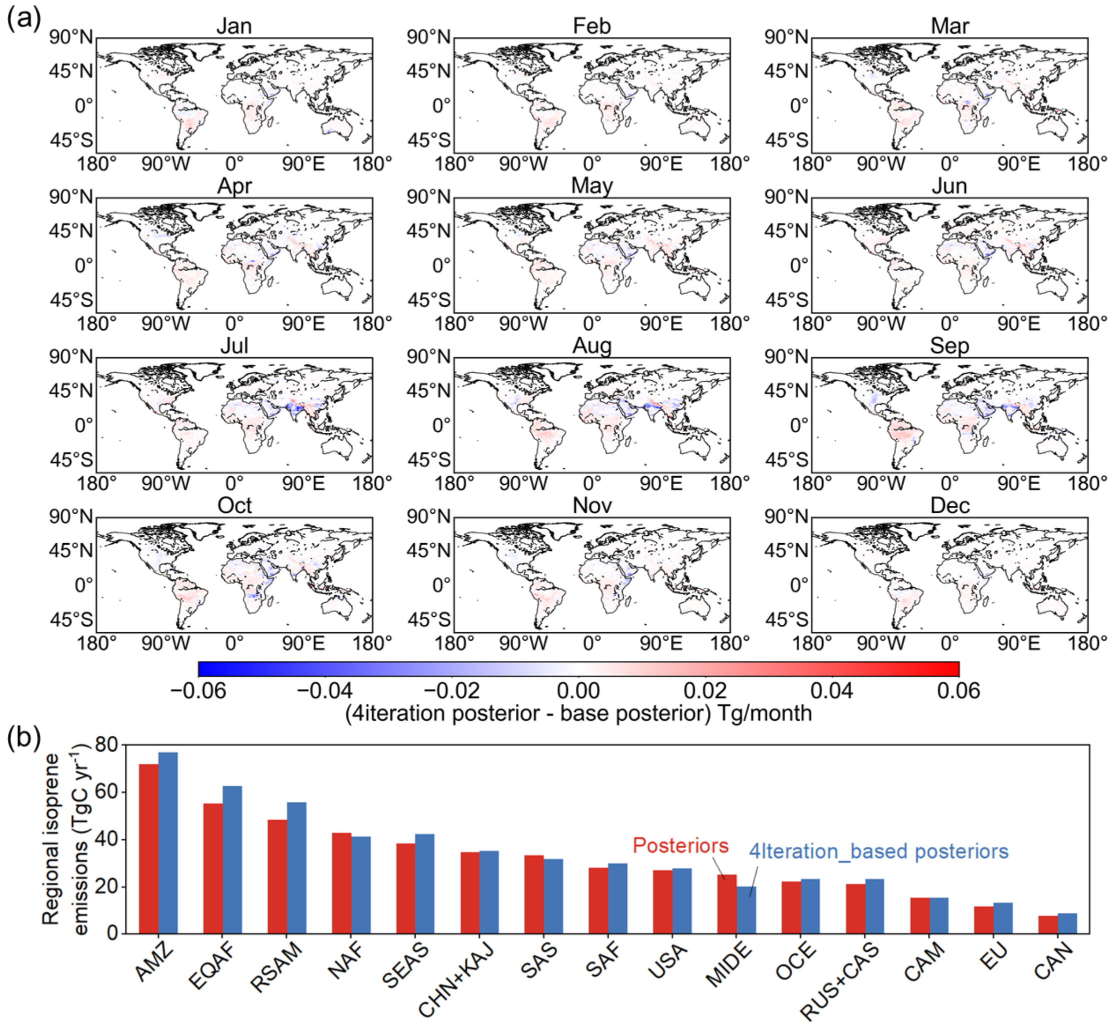

Figure S10. Comparison between base inversion and sensitivity inversion with four-time iterations. (a) presents the global distribution of monthly difference in isoprene posteriors, and (b) compares the regional annual isoprene posteriors.

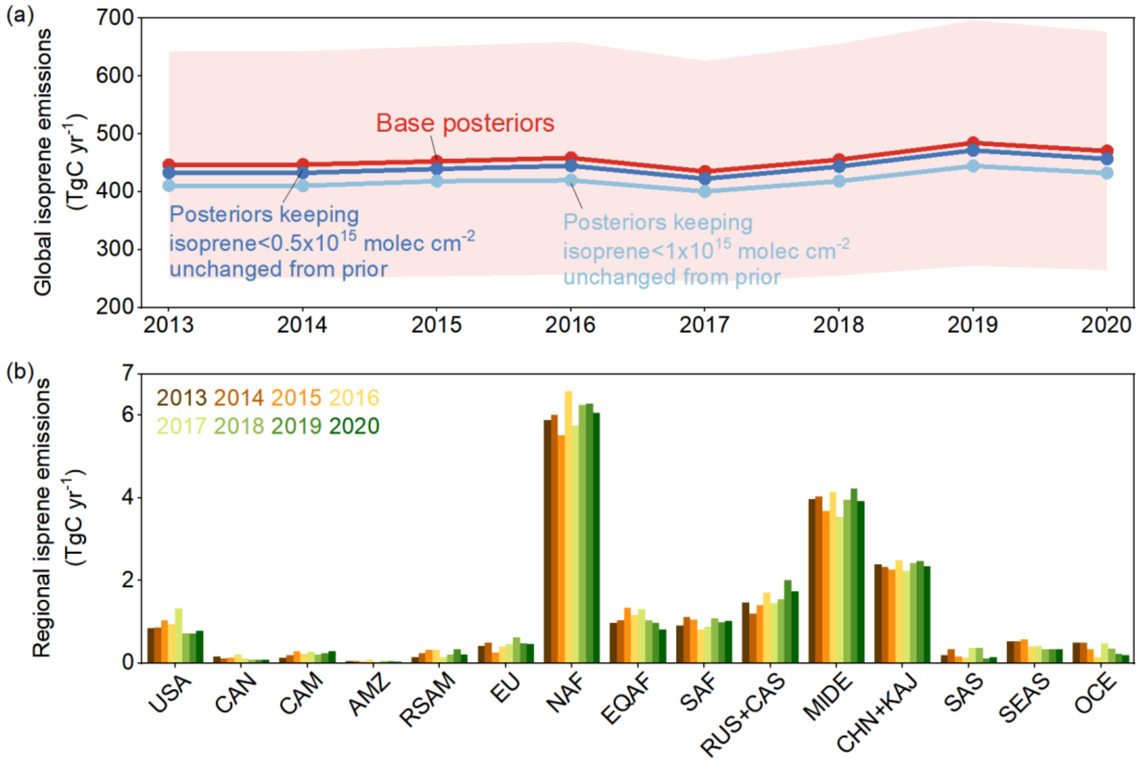

Figure S11. Comparison between base posteriors and sensitivity tests excluding grids of low isoprene columns, less than $1\text{x}10^{15}$ molec cm^{-2} and $0.5\text{x}10^{15}$ molec cm^{-2}, respectively. (a) shows the global annual posteriors, and (b) present the one standard deviation (1σ) of regional annual emissions from three posteriors from 2013 to 2020.

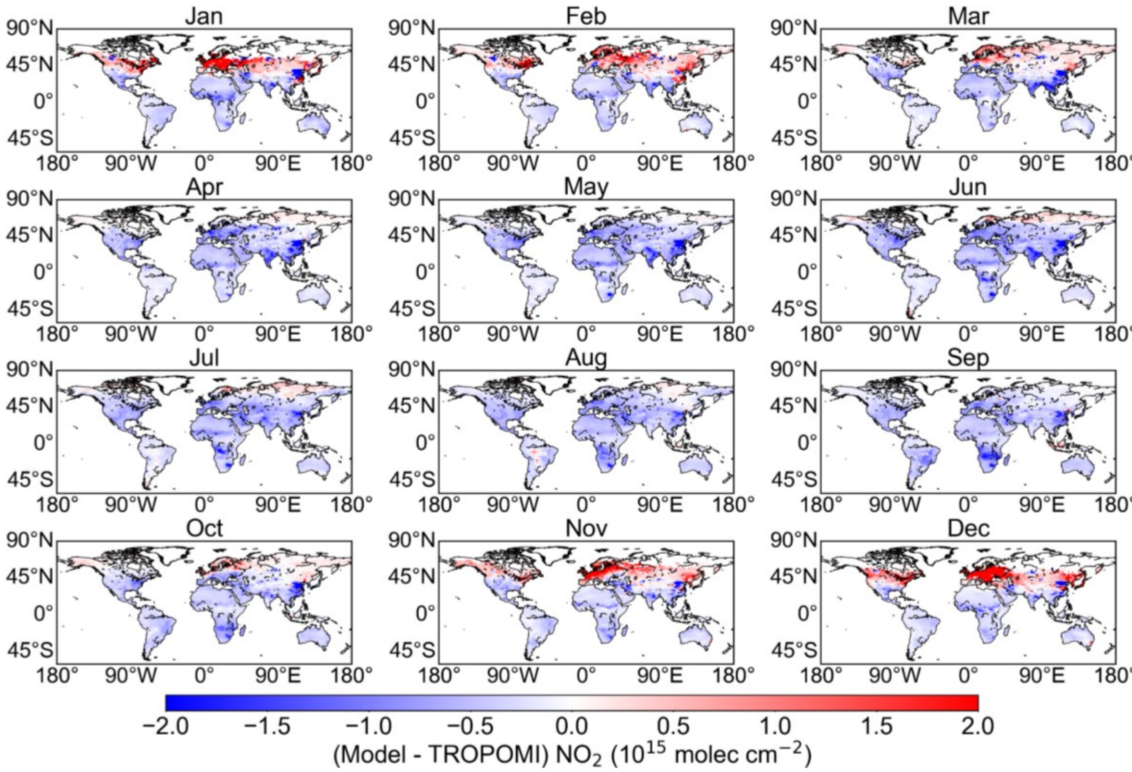

Figure S12. Comparison of LMDZ-INCA simulated NO_2 with TROPOMI observed NO_2 column concentration in 2019. Here the modeled NO_2 concentration has been resampled at TROPOMI overpass time and recalculated as model equivalence, the same as HCHO process.

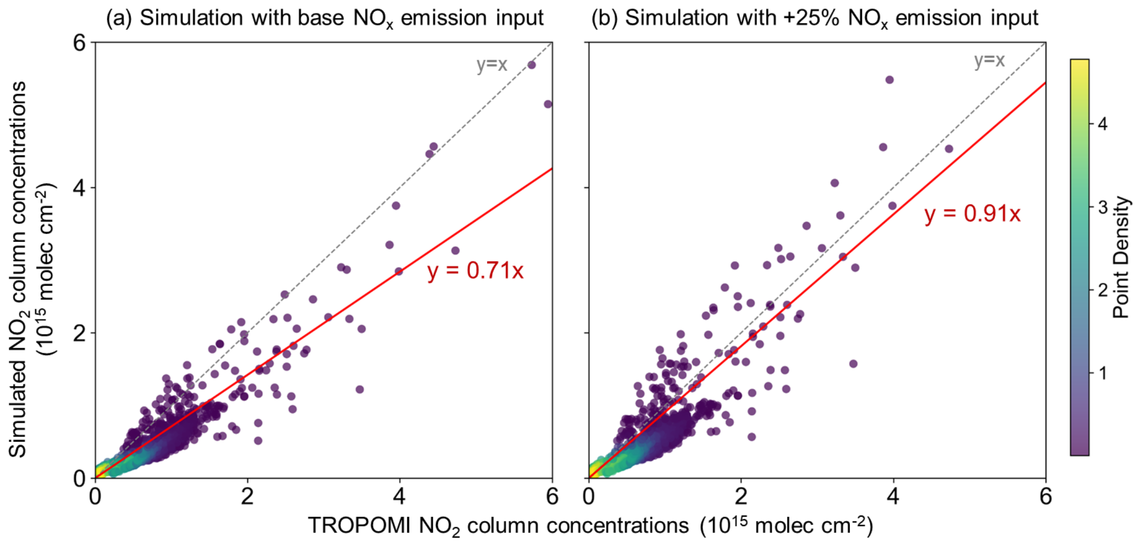

Figure S13. Correlation of LMDZ-INCA simulated NO_2 with TROPOMI observed NO_2 column concentration for (a) base CEDS NO_x and (b) +25% NO_x emissions, colored by the grid density.

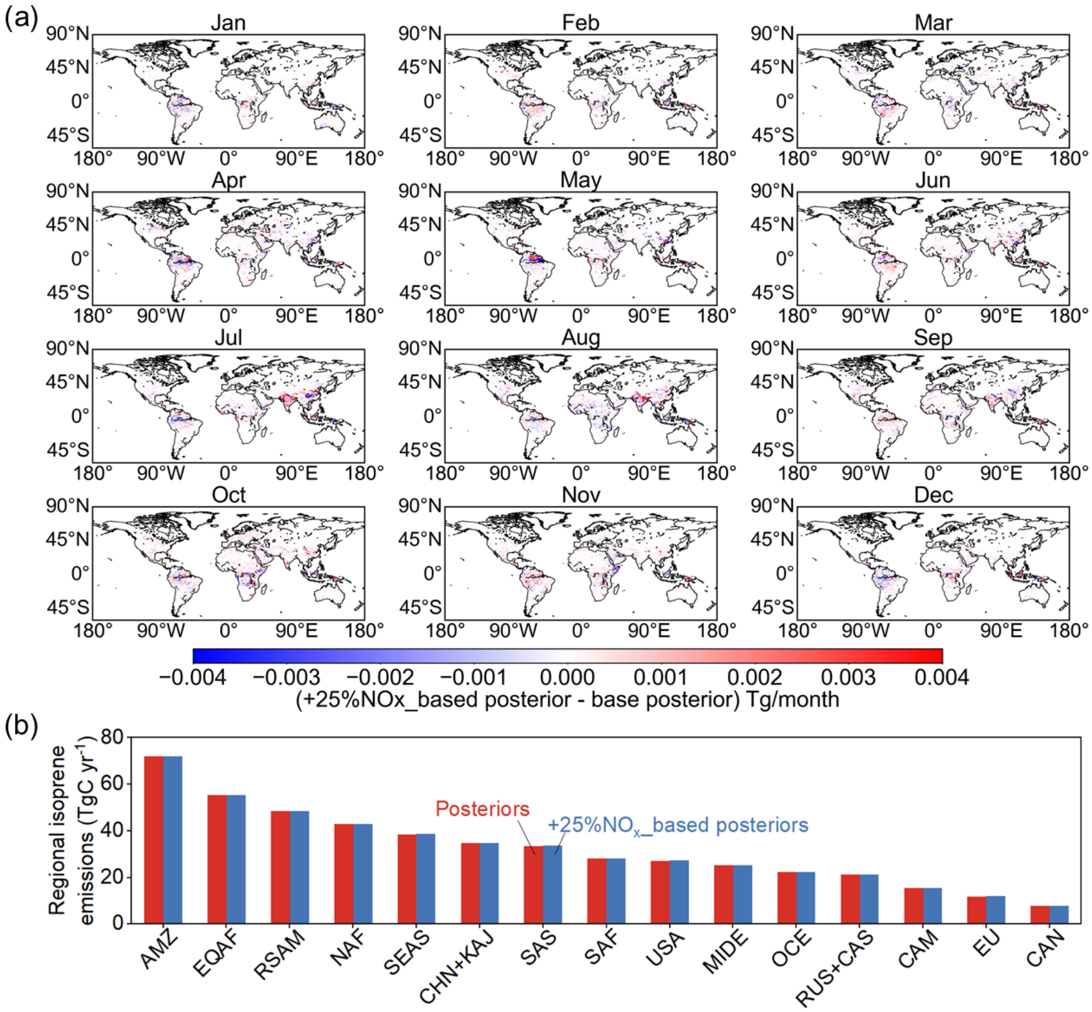

Figure S14. Comparison between base inversion and sensitivity inversion with +25% NO_x emission input. (a) presents the global distribution of monthly difference in isoprene posteriors, and (b) compares the regional annual isoprene posteriors.

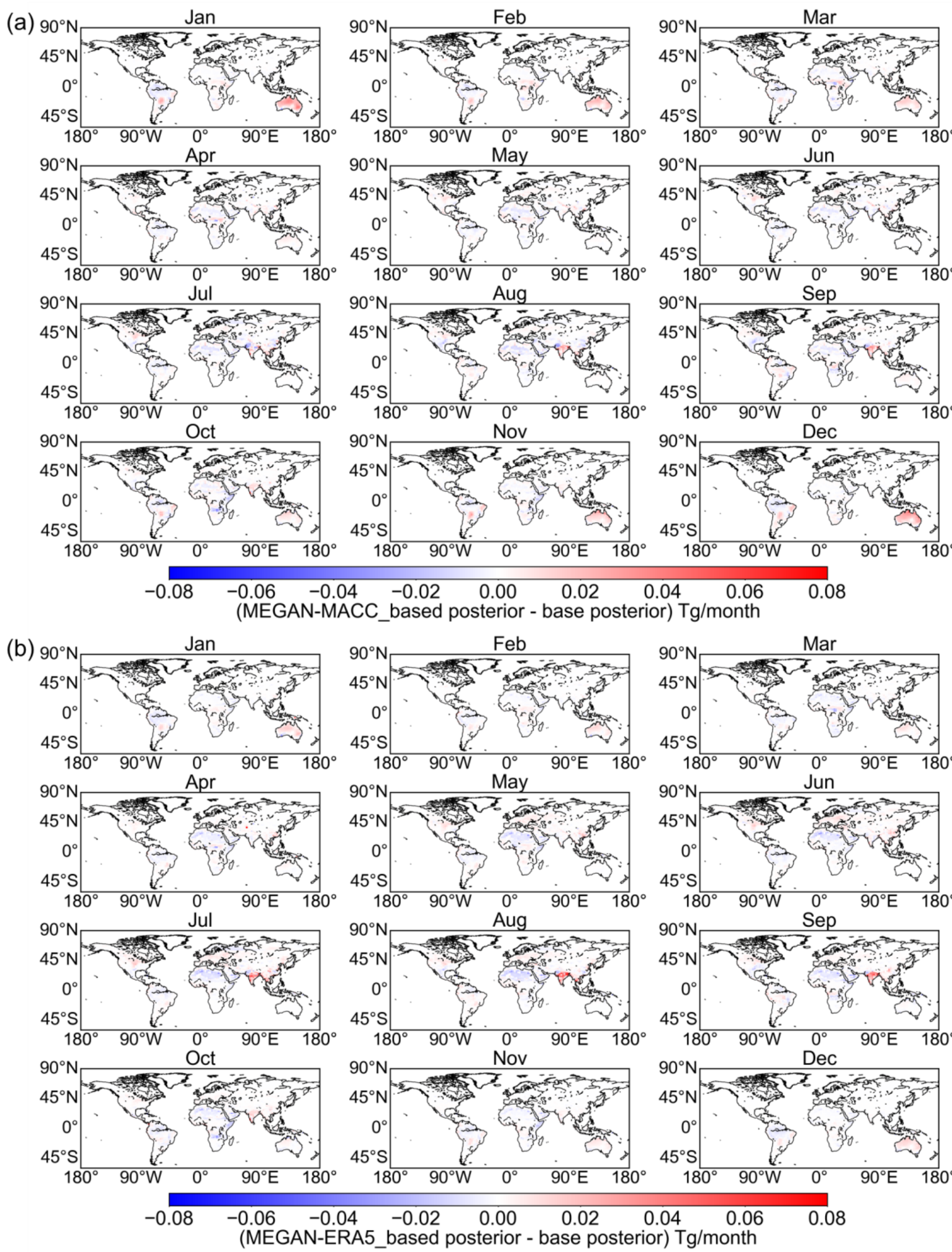

Figure S15. Monthly difference between MEGAN-MACC and MEGAN-ERA5 based posteriors and base posteriors (ORCHIDEE prior based) in 2019.

74

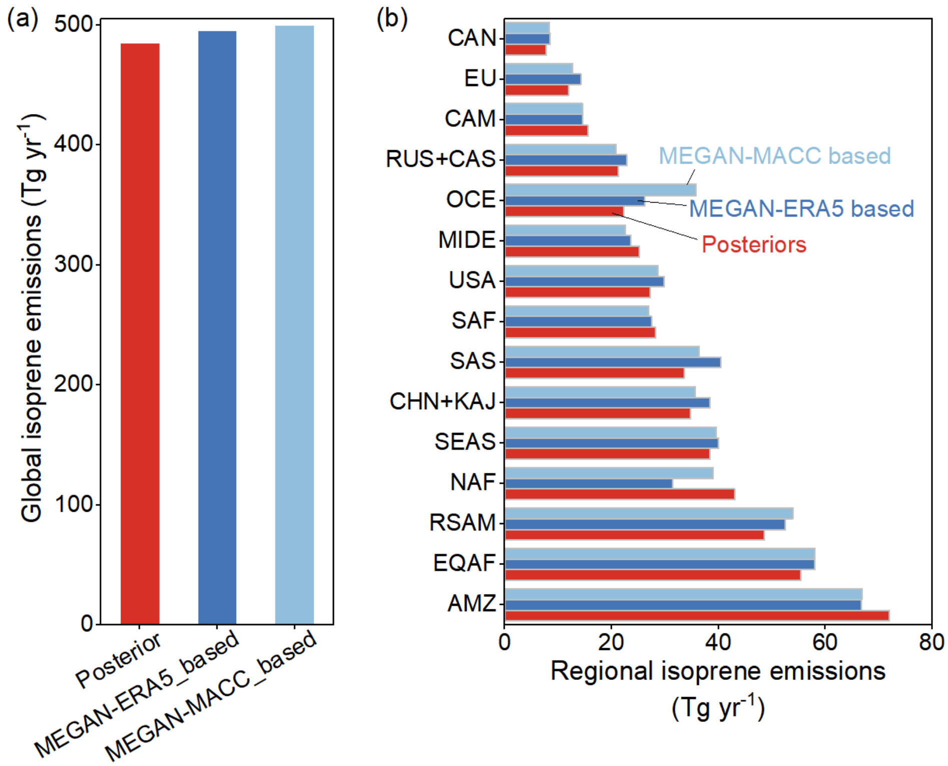

75 **Figure S16**. Comparison of three prior (ORCHIDEE, MEGAN-MACC, and MEGAN-ERA5) based
76 isoprene posteriors for (a) global and (b) regional totals in 2019.

77

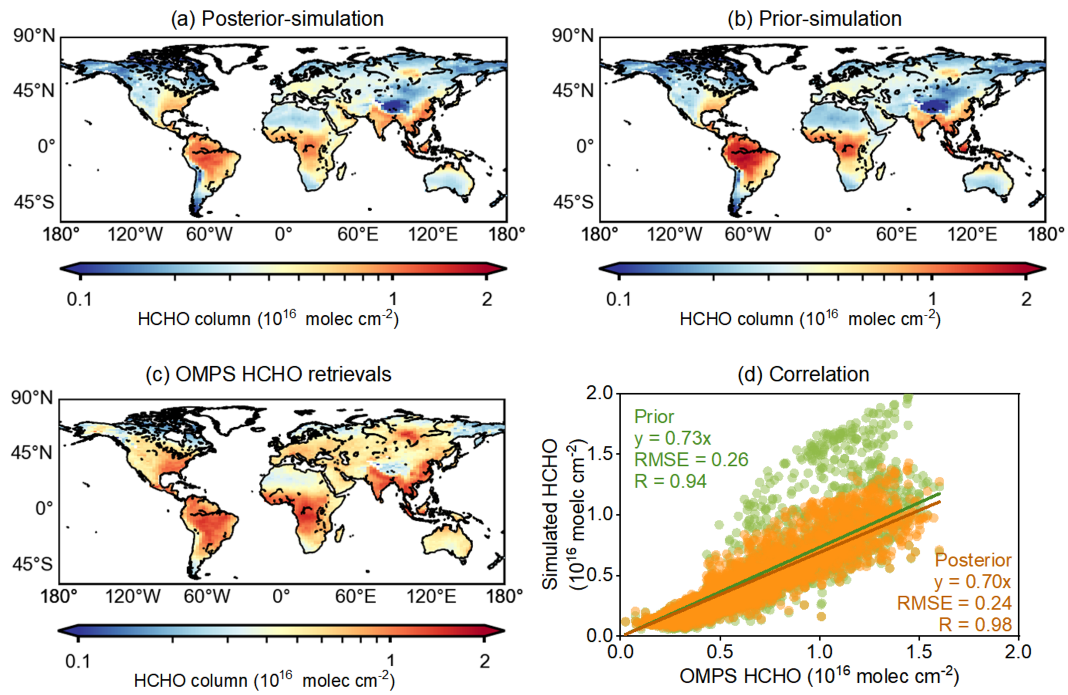

Figure S17. Comparison of simulated HCHO with OMPS observed HCHO column concentration.

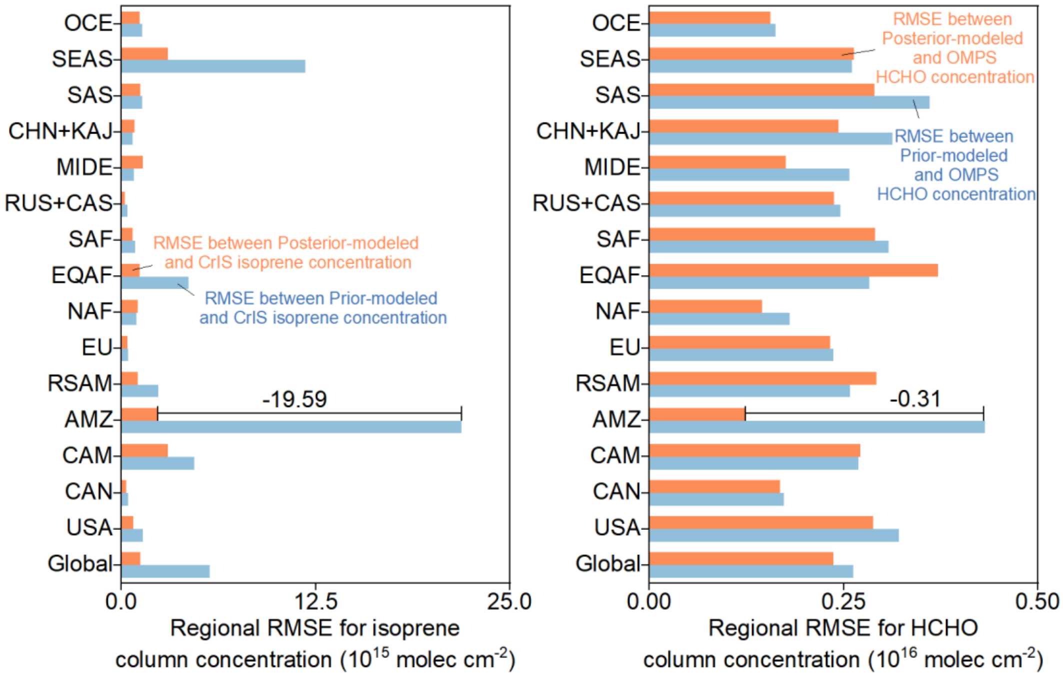

Figure S18. Global and regional Root Mean Squared Error (RMSE) for isoprene (left panel) and HCHO (right panel) column concentrations.

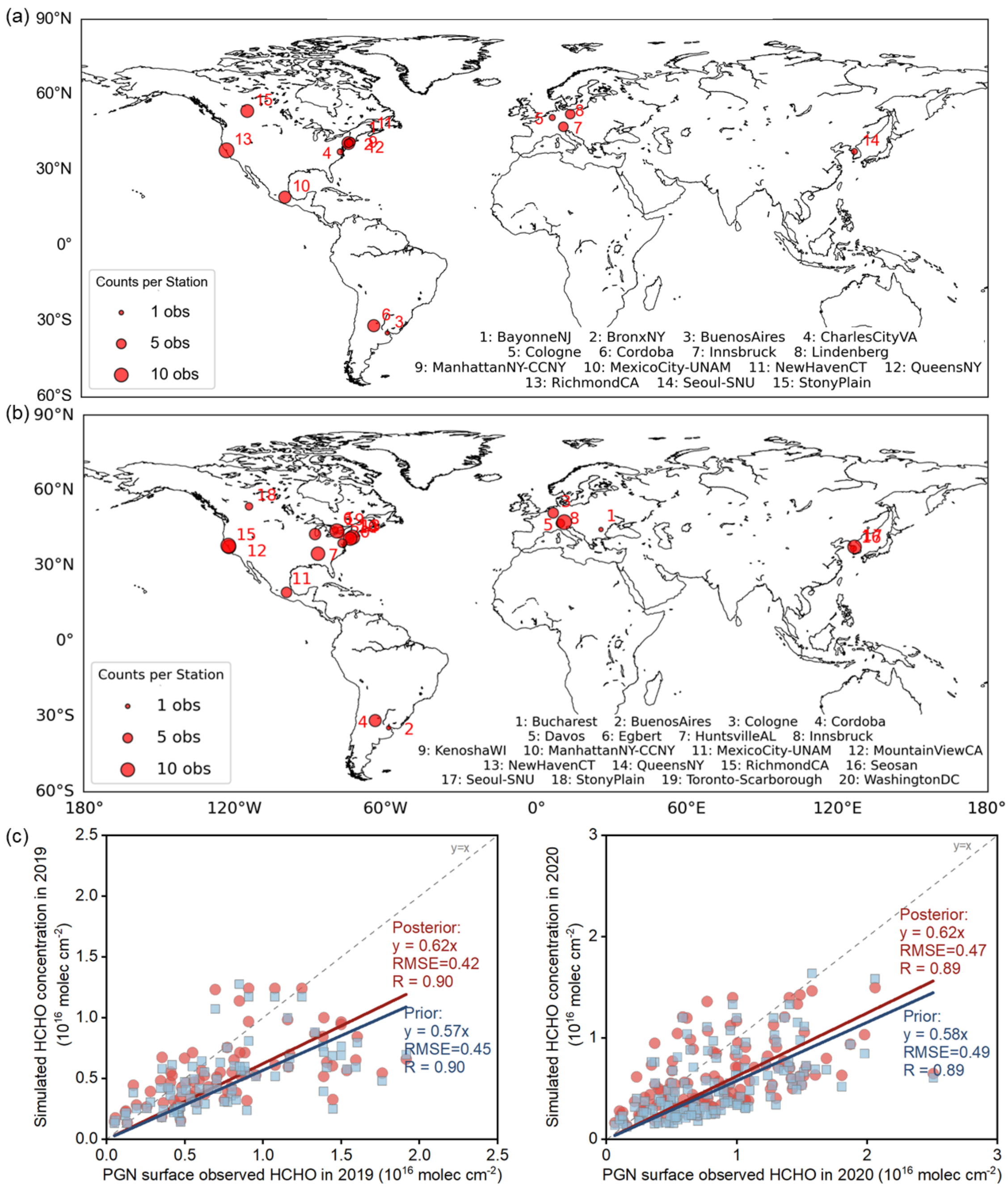

Figure S19. Comparison of HCHO column concentration between simulation and PGN surface observation in 2019 and 2020. (a) and (b) show the distribution of PGN stations used in this study, which provided official data within 60°S and 60°N for 2019 and 2020, respectively. (c) compares the correlation between posterior simulated, prior simulated, and PGN observed HCHO column concentrations in 2019 and 2020, respectively. PGN data are acquired from https://www.pandonia-global-network.org/.

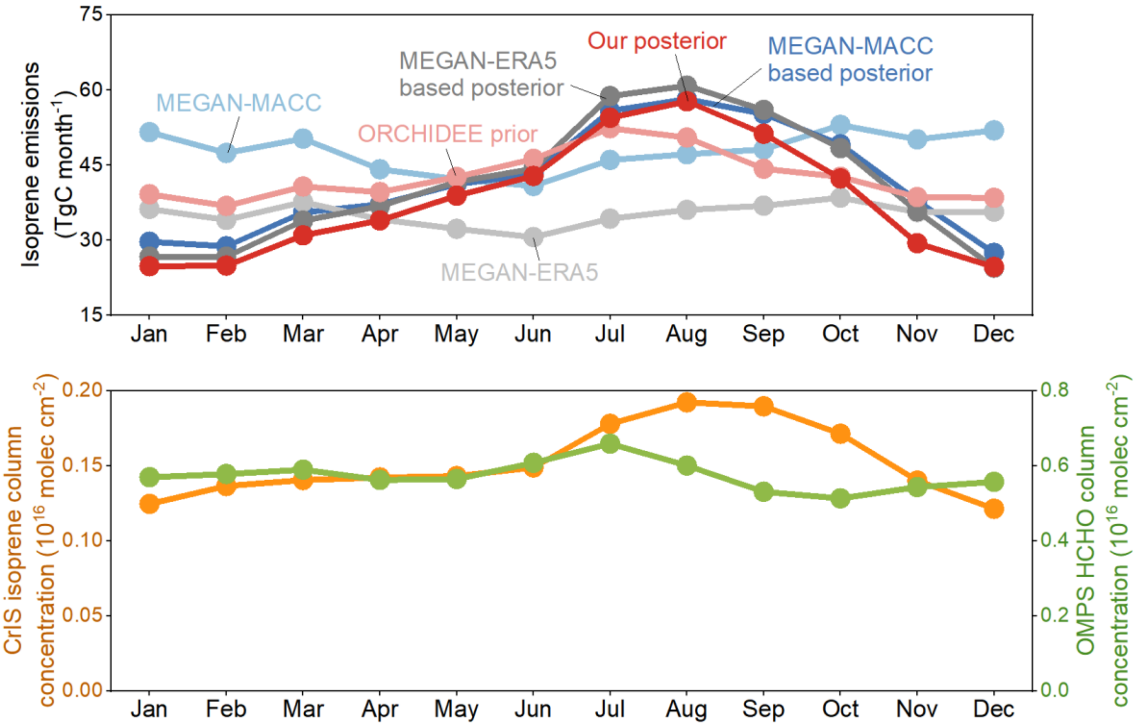

Figure S20. Monthly variation of isoprene emissions (ORCHIDEE prior and posterior, MEGAN-MACC prior and posterior, MEGAN-ERA5 and posterior) and CrIS observed isoprene column and OMPS HCHO column concentrations.

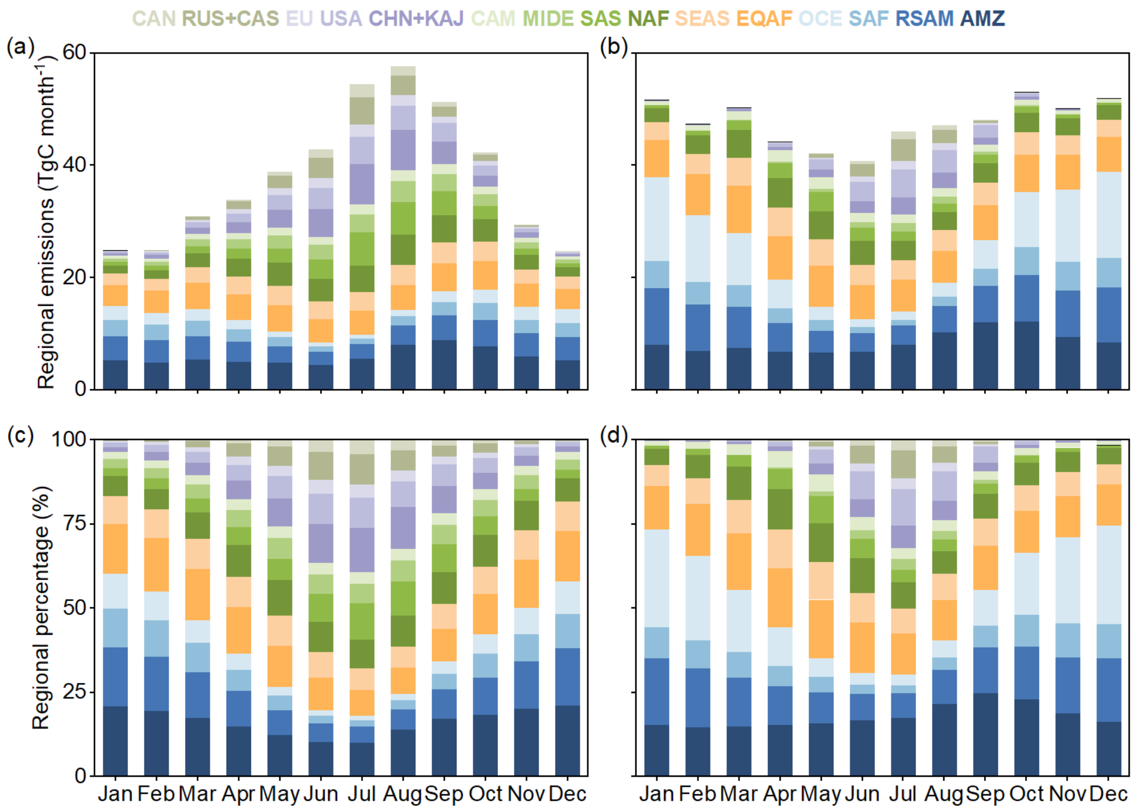

Figure S21. Comparison of regional monthly emissions between posteriors and MEGAN-MACC. (a) and (c) are the monthly absolute isoprene emissions and proportions to global totals for posteriors. (b) and (d) are the same for MEGAN-MACC inventory.

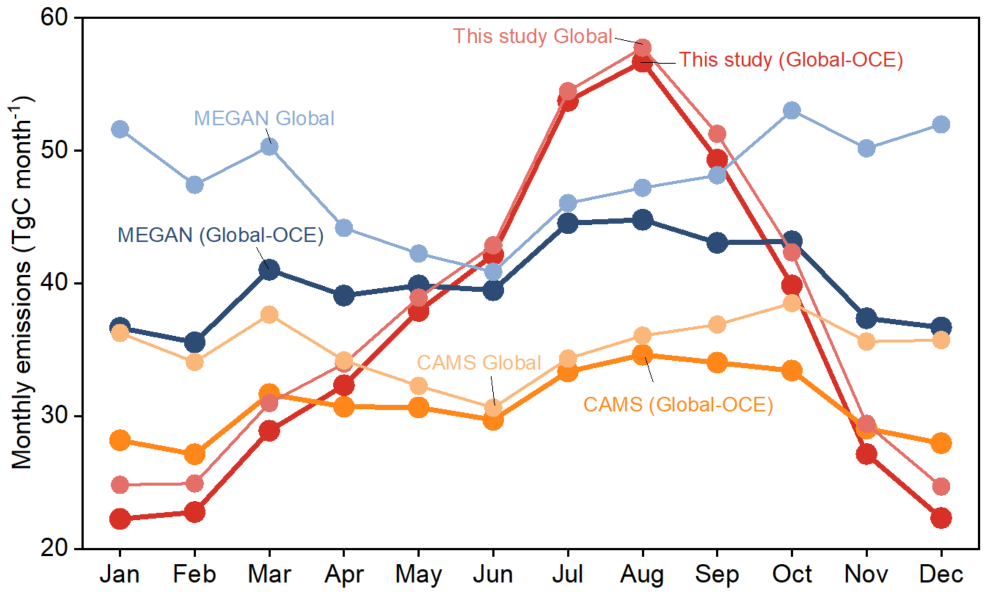

Figure S22. Comparison of seasonal patterns between posterior and inventories with and without Oceania (OCE) region.

108

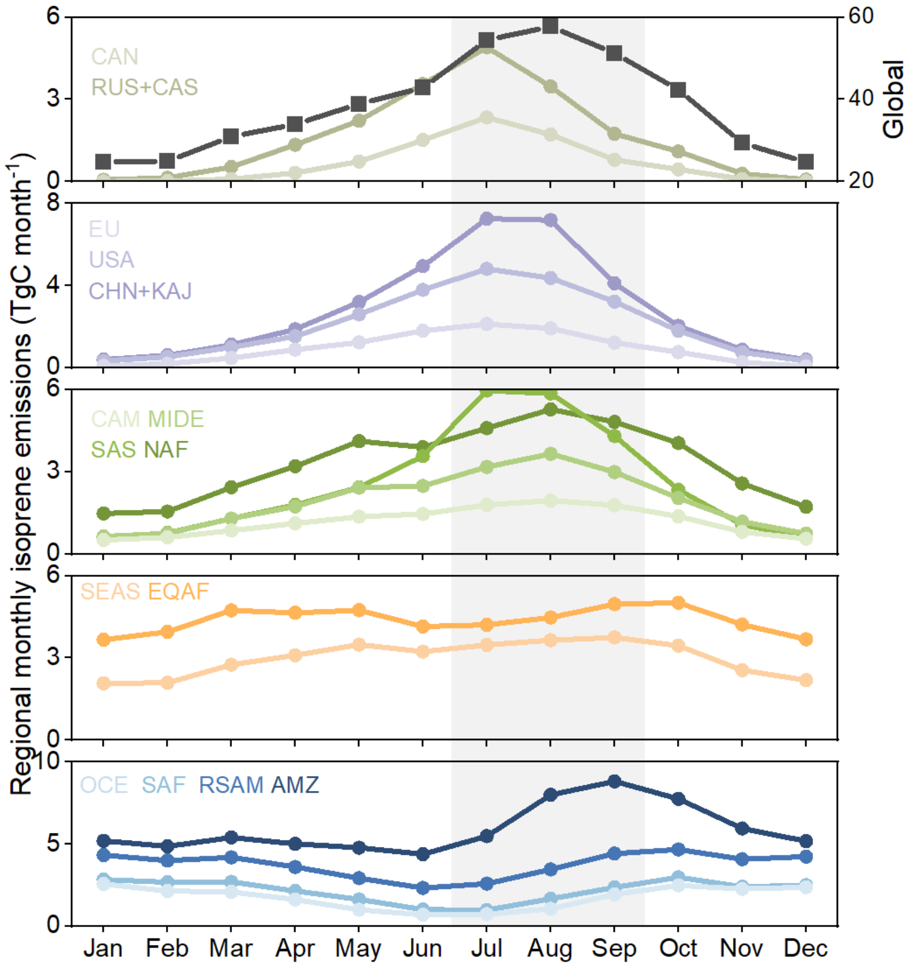

109 **Figure S23**. Monthly pattern of regional isoprene emissions averaged from 2013 to 2020.

110

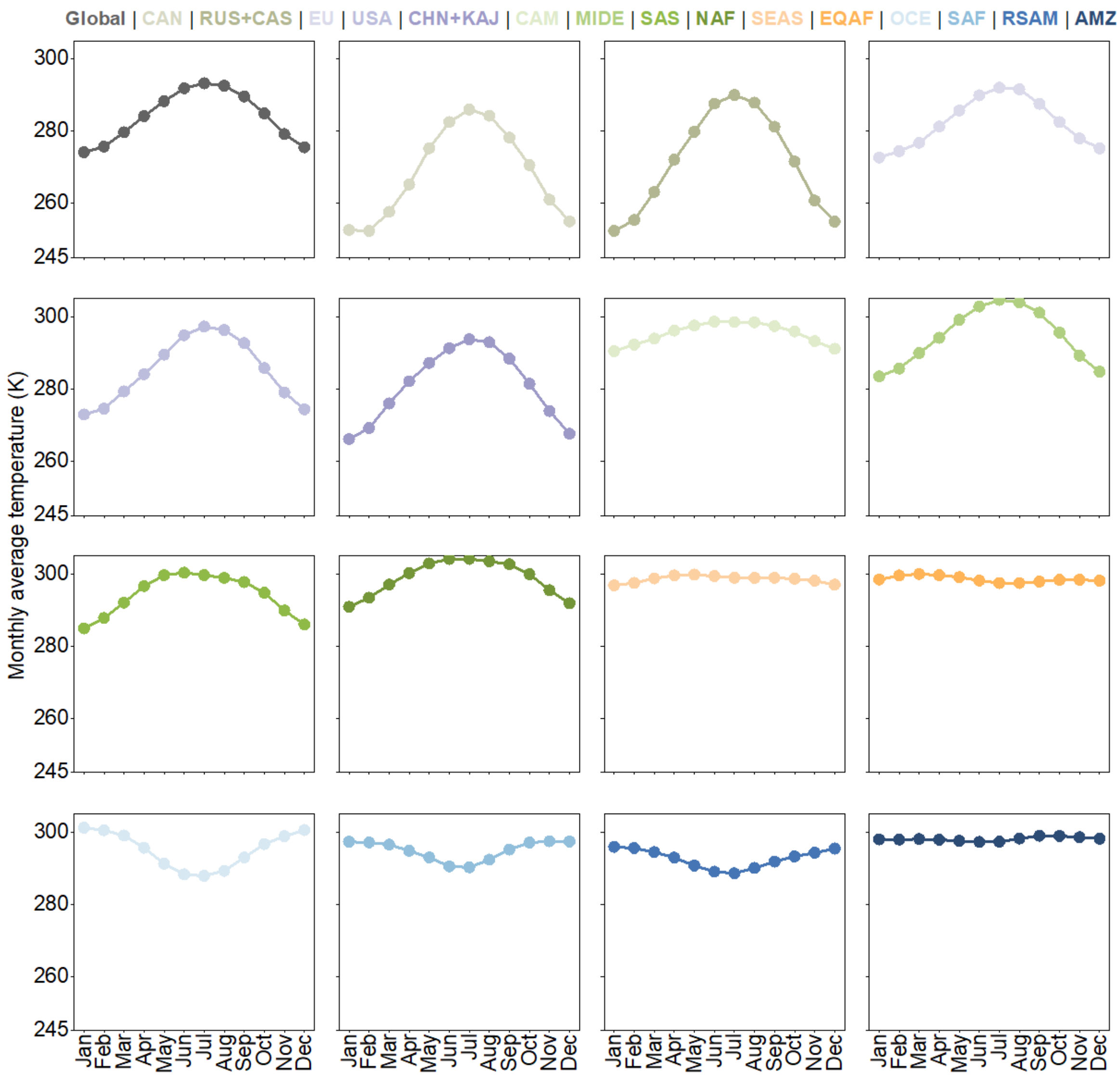

Figure S24. Global and regional monthly temperature fluctuation, with color referring regions. To highlight the fluctuation, the y-axis range are set to be the same in all panels. Data are acquired from ERA5 (https://cds.climate.copernicus.eu/datasets/reanalysis-era5-single-levels?tab=overview).

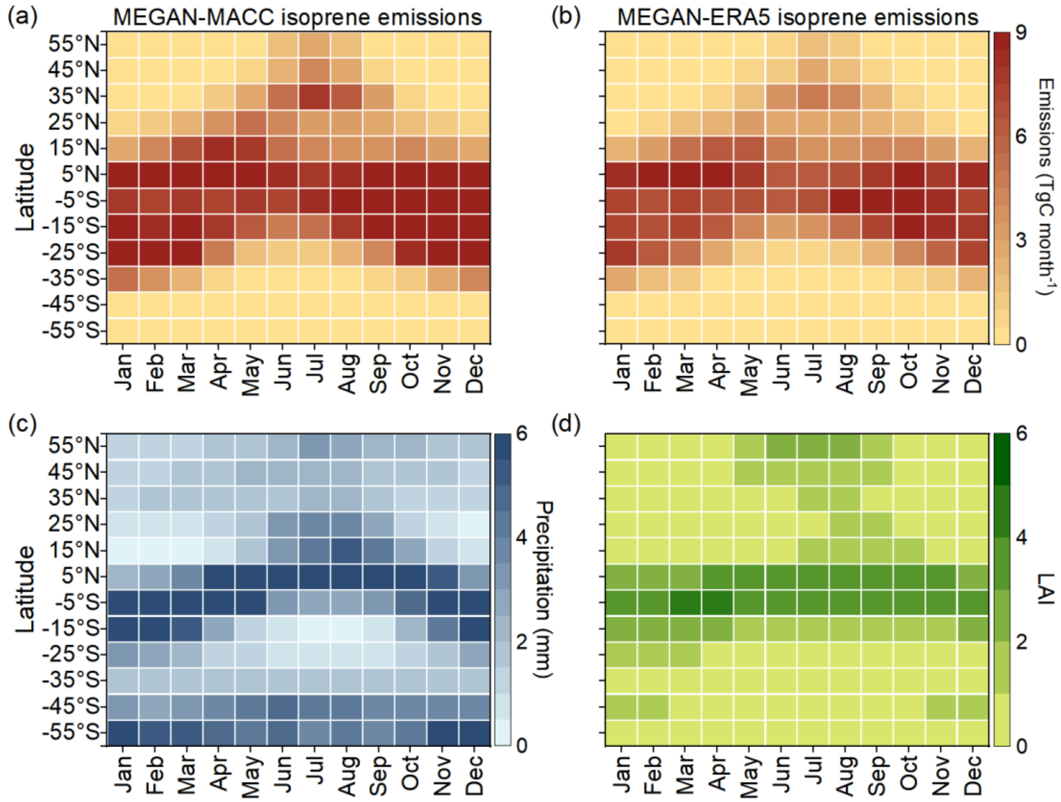

Figure S25. Monthly distributions of MEGAN-MACC and MEGAN-ERA5, precipitation, and the Leaf area index (LAI) by every 10° latitude band, respectively.

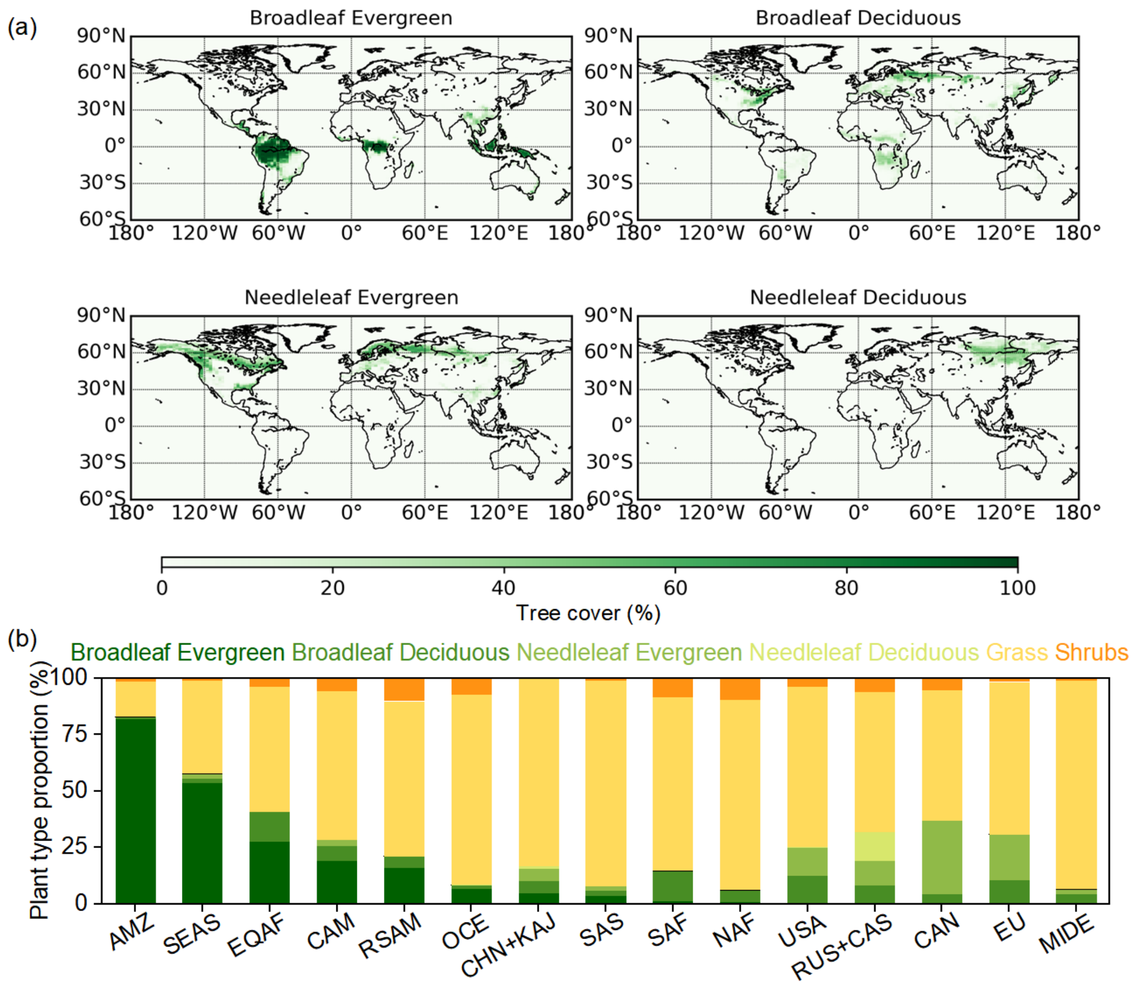

Figure S26. Distribution of plant type averaged from 2013 to 2020. (a) shows the four tress types distribution and (b) presents the percentage of all plant type in each region. Data are acquired from ESA Land Cover Climate Change Initiative (Land_Cover_cci): Global Plant Functional Types (PFT) Dataset, v2.0.8 (Li et al., 2018).

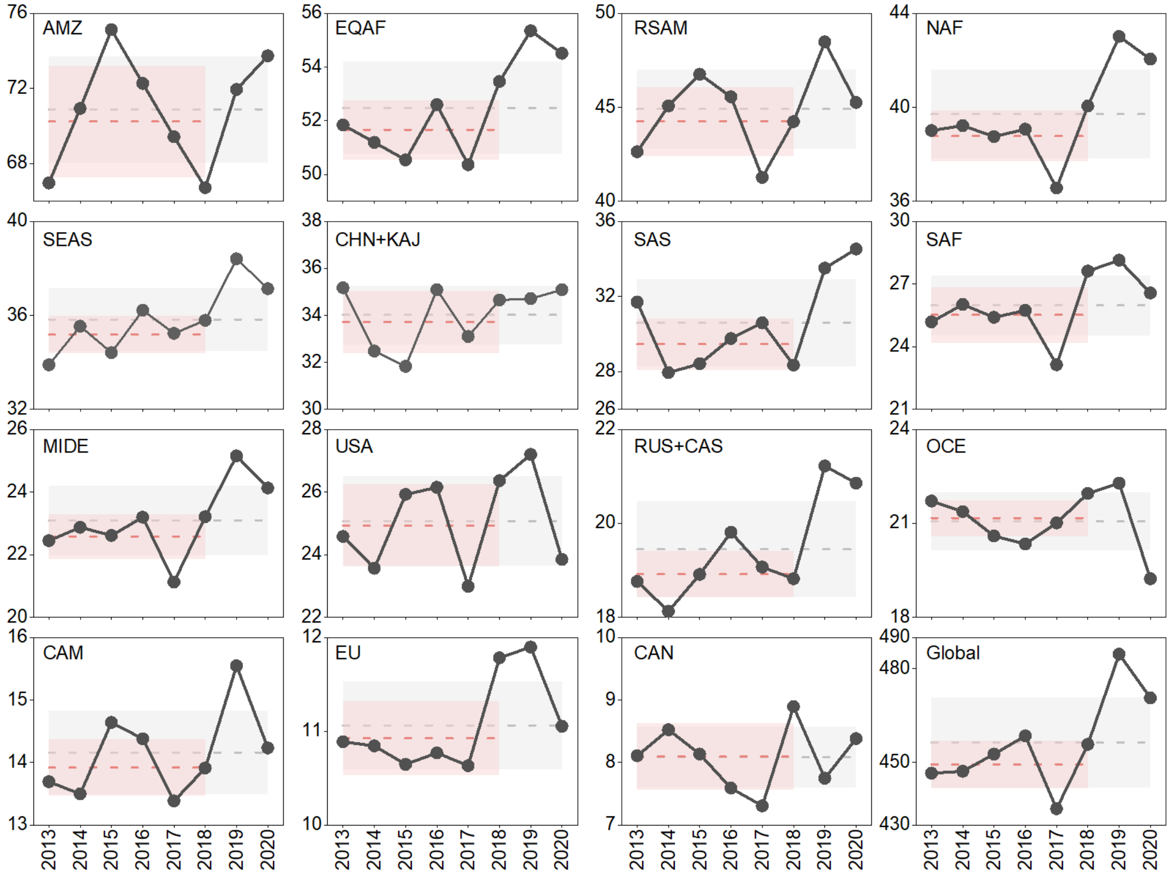

Figure S27. Annual global and regional isoprene emissions (TgC yr^{-1}) from 2013 to 2020. The gray dashed line is the annual average isoprene emissions from 2013 to 2020, and the gray shadow indicate corresponding one standard deviation (1σ). The red dashed line is the annual average isoprene emissions from 2013 to 2018, and the red shadow indicate corresponding one standard deviation (1σ).

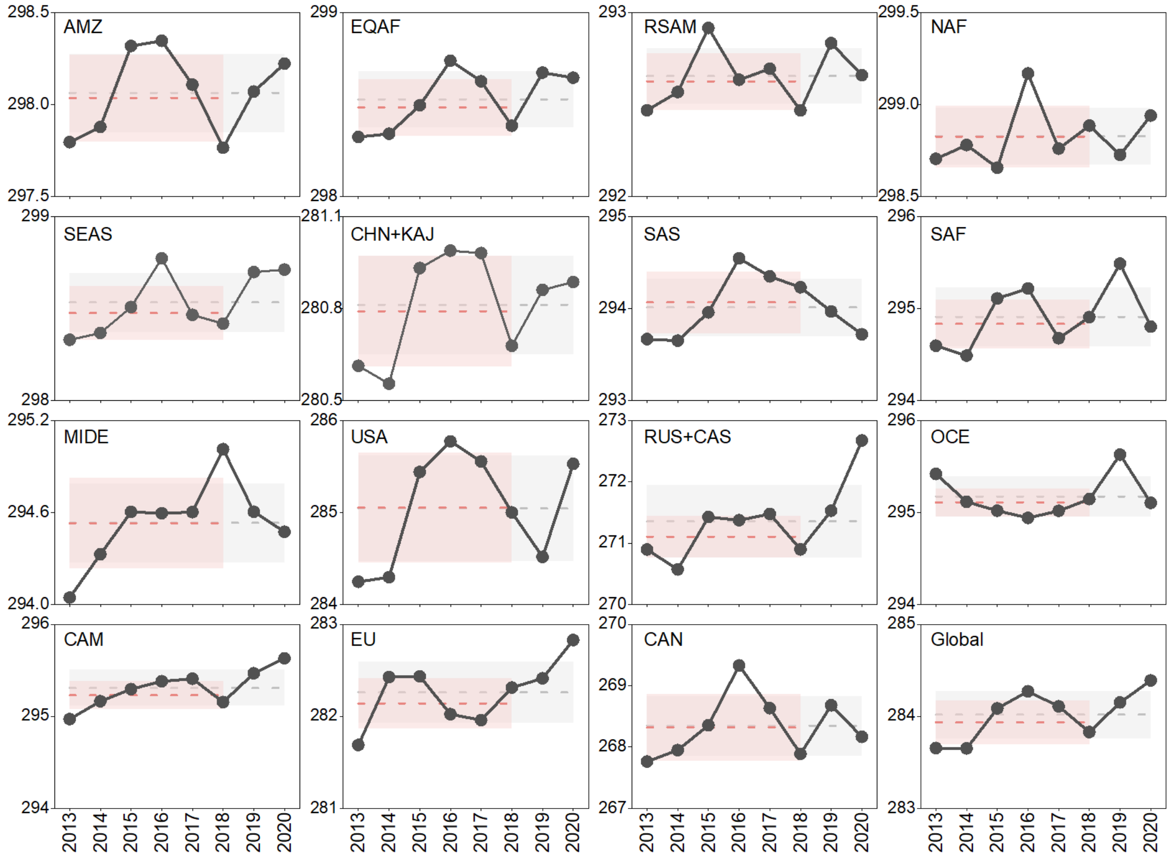

Figure S28. Regional and global annual average temperature (K) over land area from 2013 to 2020. The gray dashed line is the annual average temperature from 2013 to 2020, and the gray shadow indicate corresponding one standard deviation (1σ). The red dashed line is the annual average temperature from 2013 to 2018, and the red shadow indicate corresponding one standard deviation (1σ).

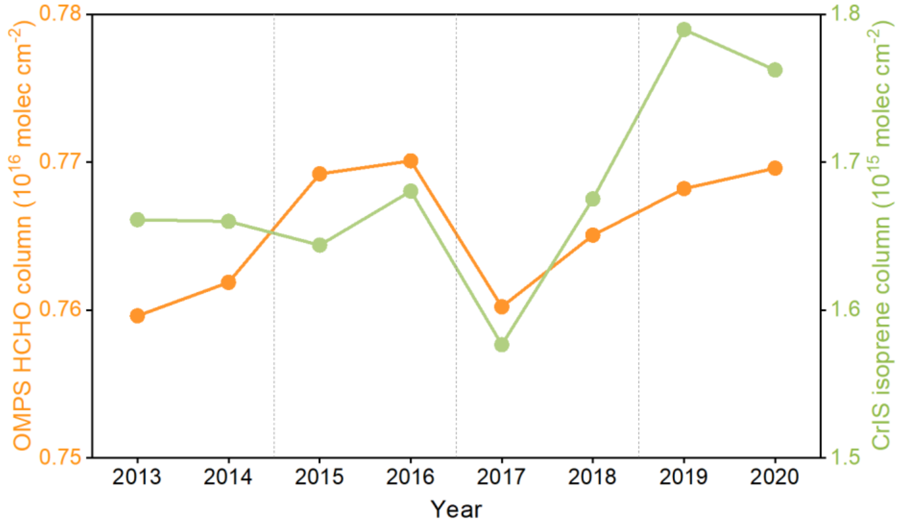

Figure S29. Annual average OMPS HCHO concentration and CrIS isoprene concentration from 2013 to 2020.

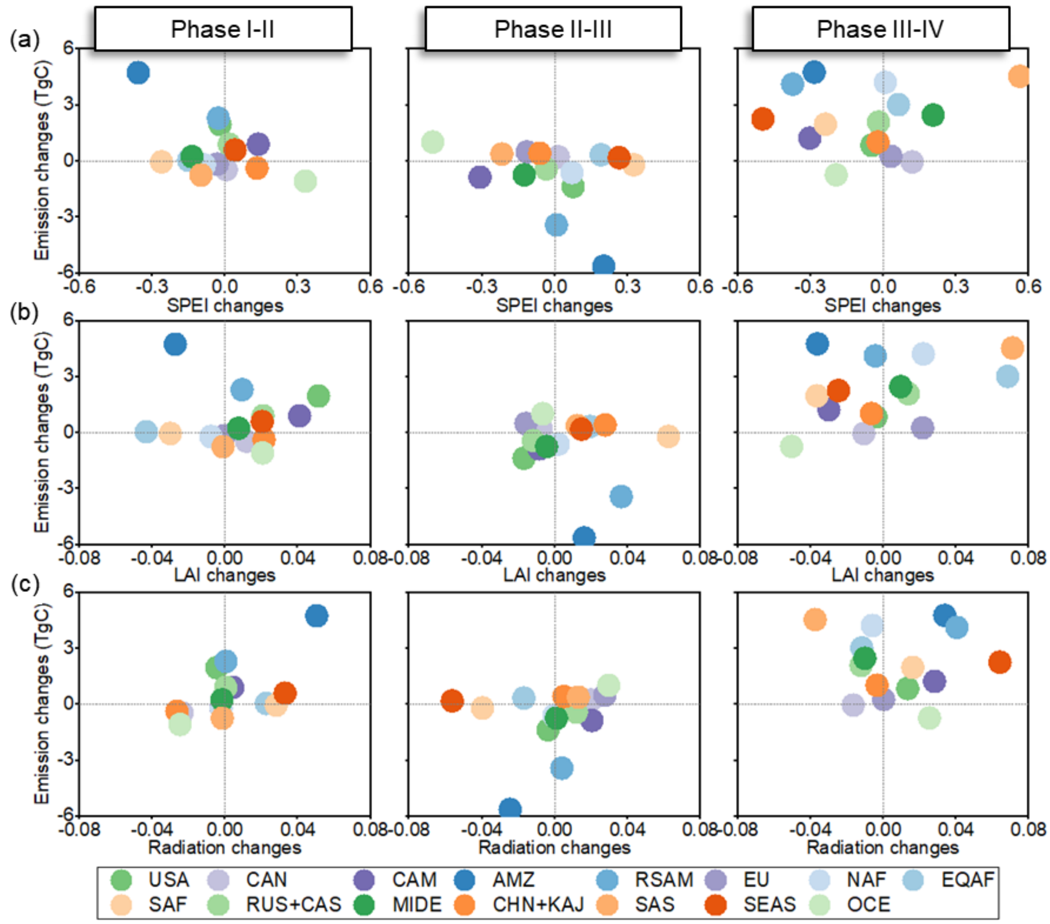

Figure S30. Correlation between the regional isoprene emission changes and (a) SPEI changes, (b) Leaf area index (LAI) changes, and (c) radiation (MJ m^{-2}) across four phases. SPEI data is from ECMWF (https://xds-preprod.ecmwf.int/datasets/derived-drought-historical-monthly?tab=overview). LAI is acquired from Pu et al. (2024).

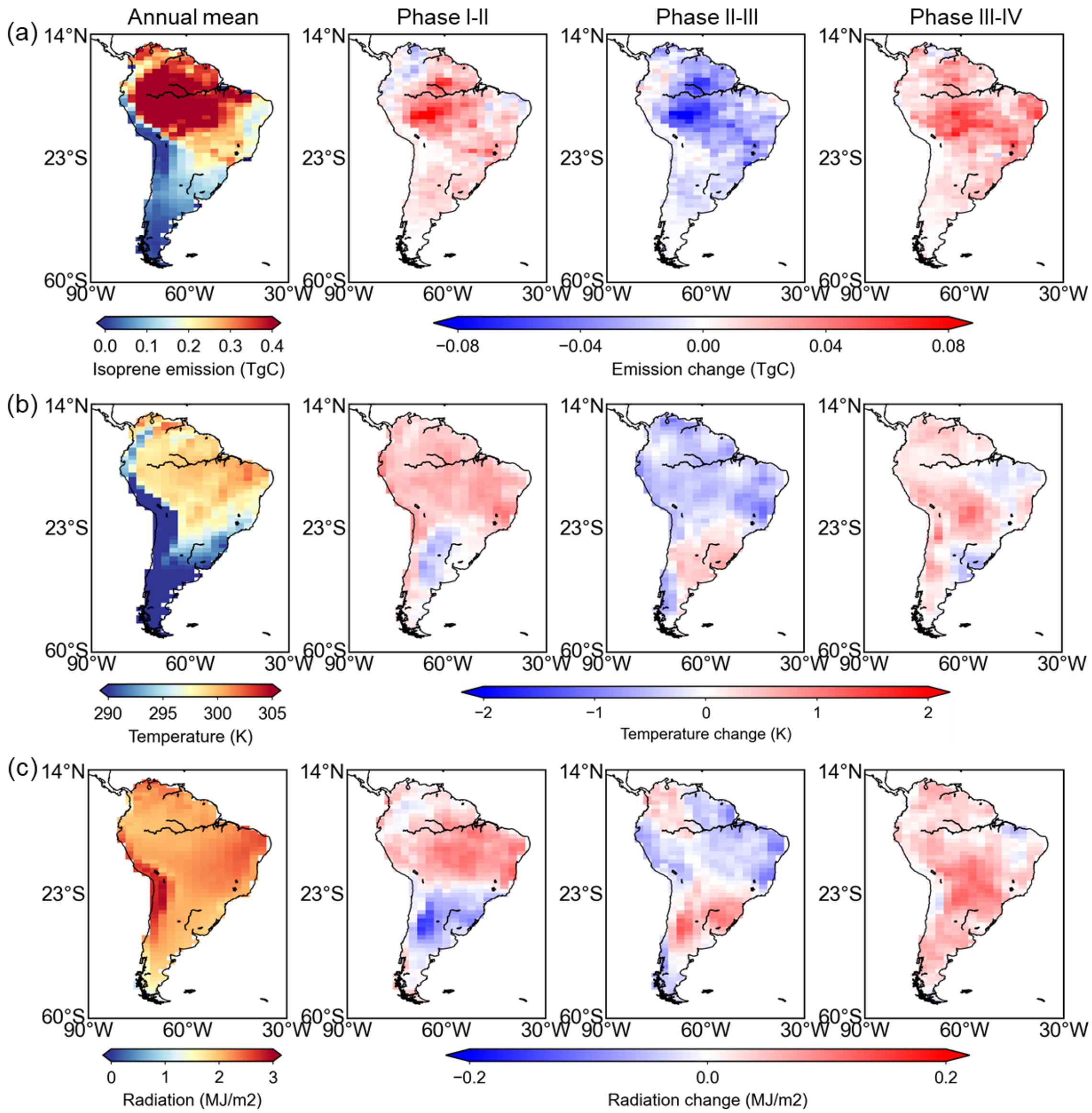

Figure S31. Regional annual mean and their changes across phases in Southern America (AMZ and RSAM) for (a) isoprene emissions, (b) temperature, and (c) radiation. The first column shows the annual mean, and the second to fourth columns correspond to the changes in regional values across phases.

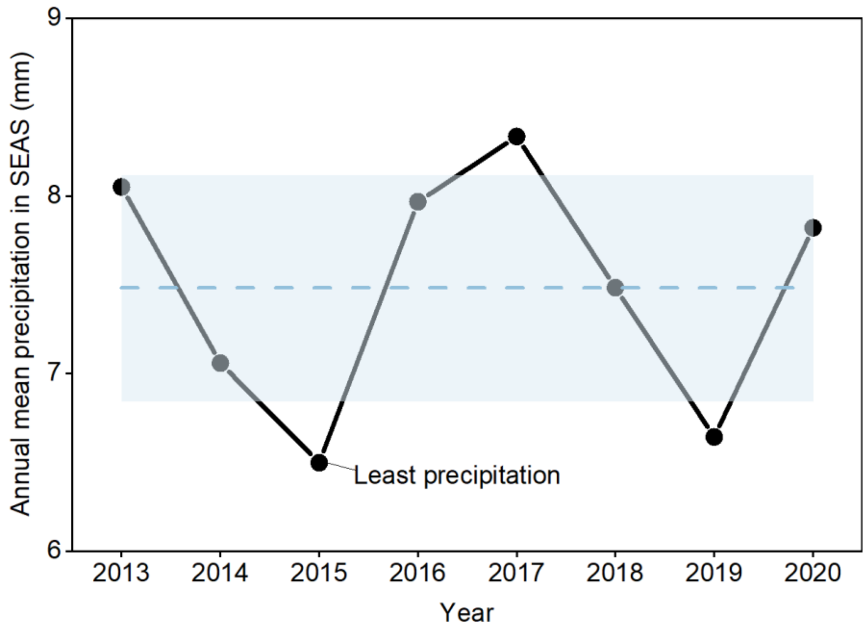

Figure S32. Annual average precipitation in SEAS from 2013 to 2020.

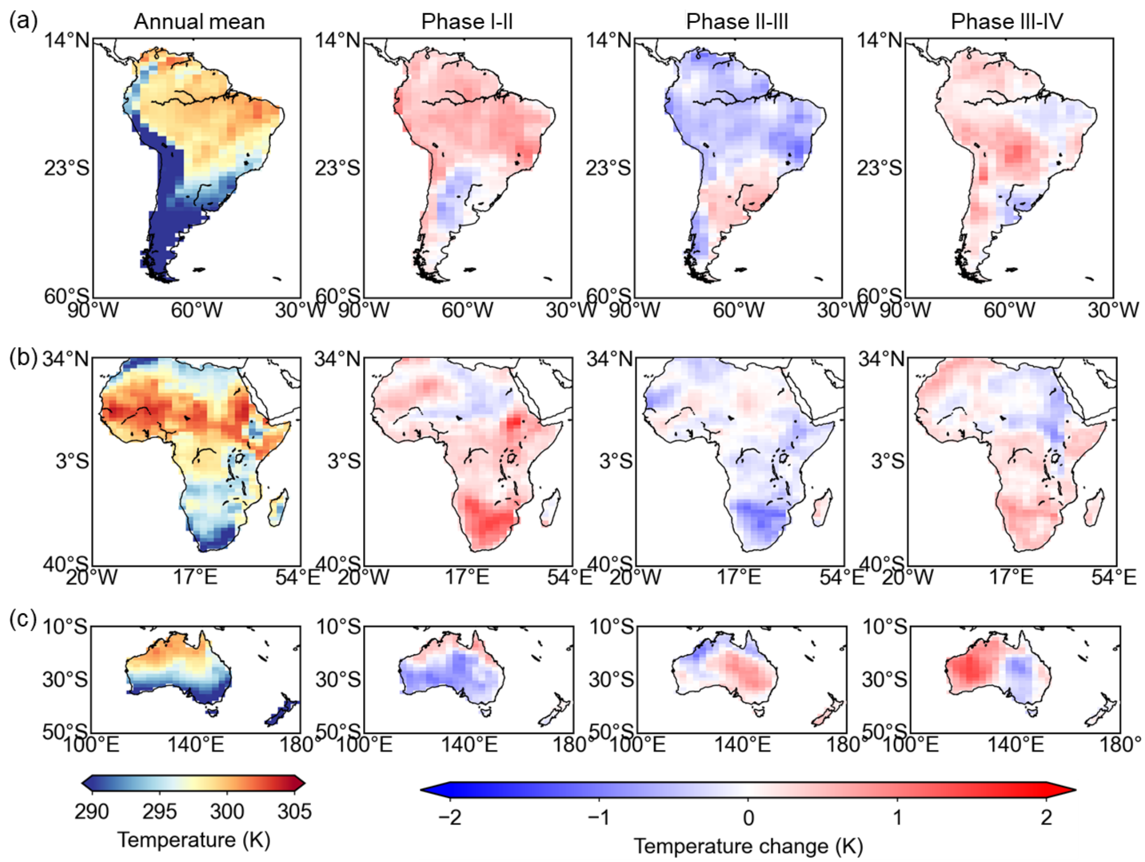

Figure S33. Regional annual average temperature and their changes across phases for (a) Southern America including AMZ and RSAM, (b) Africa including NAF, EQAF, and SAF, and (c) OCE. The first column shows the annual mean temperature for each region, and the second to fourth columns correspond to the changes in regional temperature across phases.

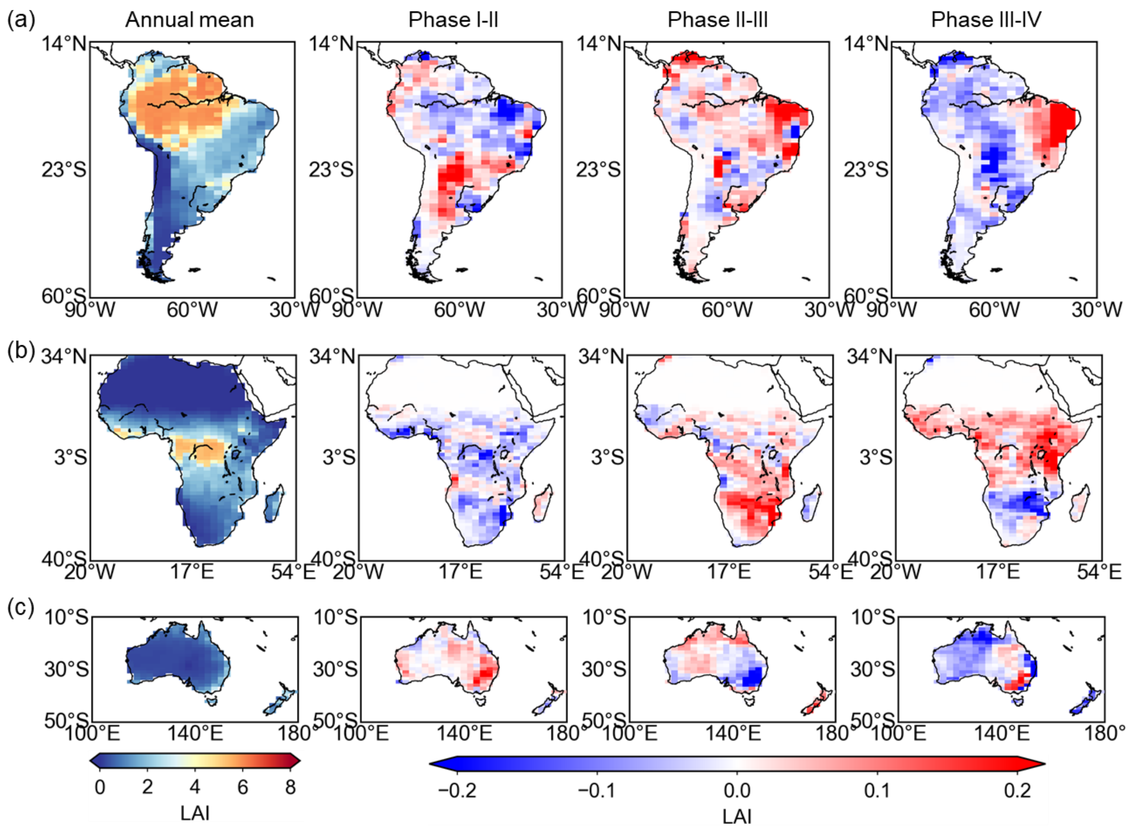

Figure S34. Regional annual average LAI and their changes across phases for (a) Southern America including AMZ and RSAM, (b) Africa including NAF, EQAF, and SAF, and (c) OCE. The first column shows the annual mean LAI for each region, and the second to fourth columns correspond to the changes in regional LAI across phases. LAI is from Pu et al. (2024).

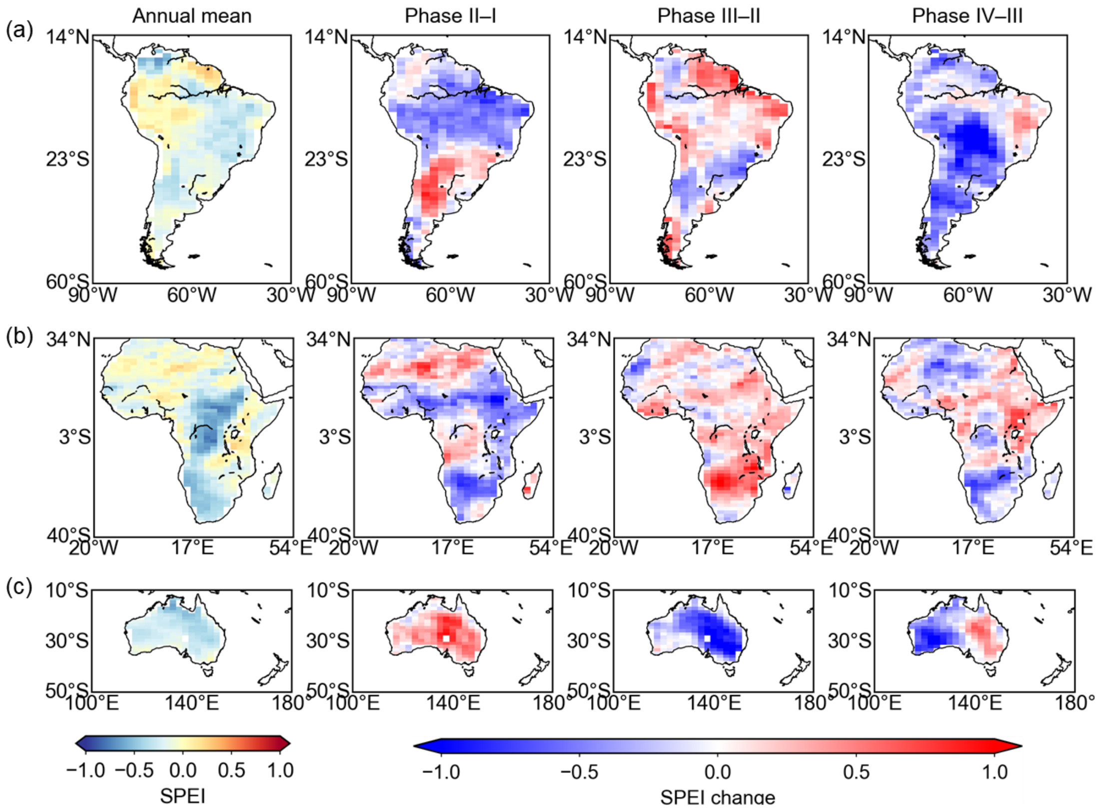

Figure S35. Regional annual average SPEI and their changes across phases for (a) Southern America including AMZ and RSAM, (b) Africa including NAF, EQAF, and SAF, and (c) OCE. The first column shows the annual mean precipitation for each region, and the second to fourth columns correspond to the changes in regional precipitation across phases.

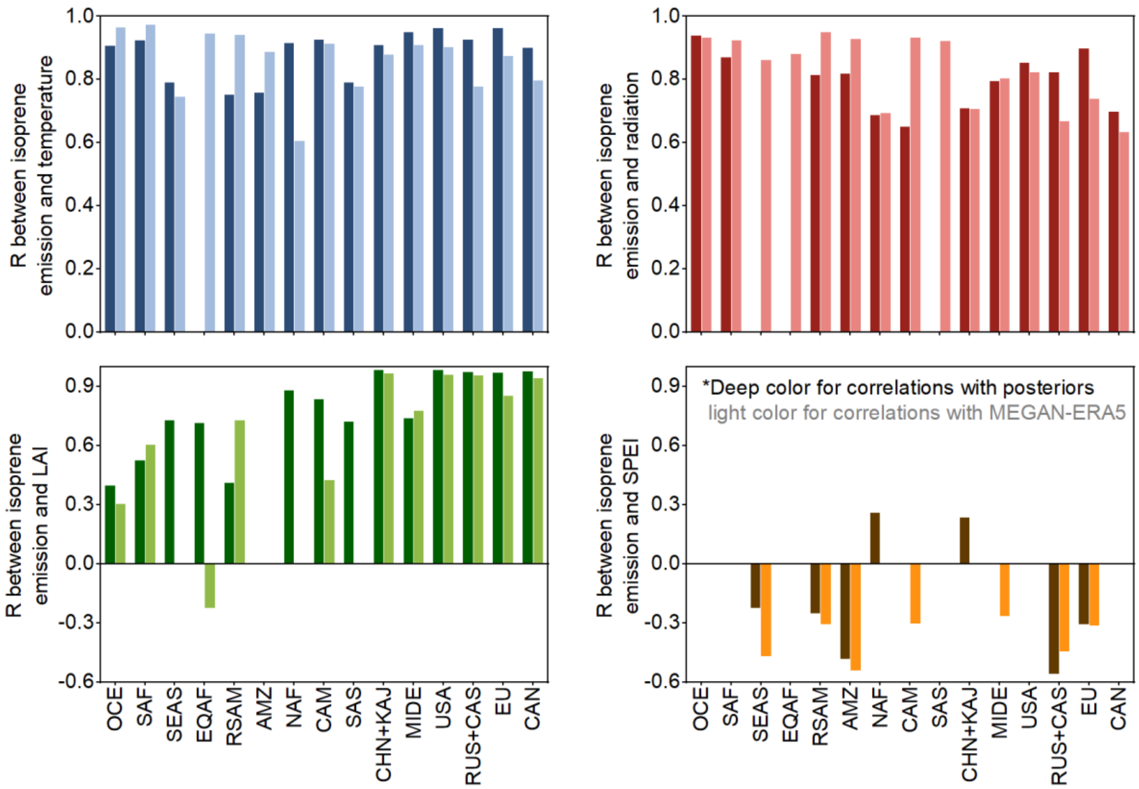

Figure S36. Comparison of the correlation coefficients (R) between isoprene emissions and environmental factors on a monthly scale for the posterior emissions from this study (deep-colored bars) and the MEGAN-ERA5 inventory (light-colored bars). Only statistically significant correlations ($p < 0.05$) are shown.

Table S1. Overview of isoprene-related chemistry in LMDZ-INCA model.

N	Isoprene-related reactions	Rate coefficient
1	ISOPOOH+ hv → 0.402MVK + 0.288MACR + 0.69CH2O + HO2	-
2	ISOP + OH → ISOPO2	3.0e-11exp(360/T)
3	ISOP + NO3 → ISOPNO3	3.5e-12exp(-450/T)
4	ISOPO2 + HO2 → ISOPOOH	8.e-13exp(700/T)
5	ISOPOOH + OH → 0.8XO2 + 0.2ISOPO2	1.52e-11exp(200/T)
6	ISOP + O3 → 0.42MACR + 0.16MVK + 0.18OH + 0.05C3H6 + 0.42CH2O + 0.27CO + 0.09HO2 + 0.44O3OLSB + 0.07H2 + 0.15CO2	11.01e-15exp(-2000/T)
7	ISOPO2 + NO → 0.08ONITR + 0.92NO2 + 1.0HO2 + 0.32MVK + 0.51CH2O + 0.23MACR + 0.37HYDRALD	4.4e-12exp(180/T)
8	ISOPO2 + NO3 →1.0HO2+ 0.6CH2O + 1.0NO2 + 0.25MACR + 0.35MVK + 0.4HYDRALD	2.40e-12
9	ISOPO2 + CH3O2 → 0.25CH3OH + 1.0HO2 + 1.2CH2O + 0.19MACR+ 0.26MVK+ 0.3HYDRALD	5.0e-12exp(400/T)
10	ISOPO2 + CH3CO3 → 1.0CH3O2 + 1.0HO2 + 0.6CH2O + 0.25MACR+ 0.35MVK + 0.40HYDRALD	14.00e-12
11	ISOPNO3 + NO → 1.206NO2 + 0.794HO2 + 0.072CH2O + 0.167MACR + 0.039MVK + 0.794ONITR	2.7e-12exp(360/T)
12	ISOPNO3 + NO3 → 1.206NO2 + 0.794HO2 + 0.072CH2O + 0.167MACR + 0.039MVK + 0.794ONITR	2.40e-12
13	ISOPNO3 + HO2 → 1.0XOOH + 0.206NO2 + 0.794HO2 + 0.008CH2O + 0.167MACR + 0.039MVK + 0.794ONITR	1.9e-13exp(1300/T)
14	ISOPNO3 + CH3O2 → 0.06NO2 + 0.711HO2 + 0.697CH2O + 0.059MACR + 0.001MVK + 0.635ONITR + 0.305CH3OH	1.7491e-12

* ISOPOOH (HOCH2COOHCH3CHCH2); MVK (CH2CHCOCH3); MACR (CH2CCH3CHO); ISOP (C5H8); ISOPO2 (C5H8OHO2); ISOPNO3 (nitrate radical adduction to isoprene); XO2 (counter for organic peroxy radicals); O3OLSB (secondary and generic species produced during the oxydation of alcenes); ONITR (C5H8ONO2); HYDRALD (HOCH2CCH3OOCH3CHCHO); XOOH (counter for organic hydroperoxides).

* The photolytic reaction rates refer to Madronich and Flocke (1999) and Guy and Susan (1987); Other reaction rates refer to (Burkholder et al., 2019). Table S2 also apply this data source.

Table S2. Overview of HCHO-related chemistry in LMDZ-INCA model.

N	HCHO-related reactions	Rate coefficient
1	CH2O + hv → HCO + H	-
2	CH2O + hv → CO + H2	-
3	MACR + hv → 1.34HO2 + 0.66MCO3 + 1.34CH2O + 1.34CH3CO3	-
4	GLYOXAL+ hv → CO + CH2O	-
5	ONITR + hv → HO2 + CO + NO2 + CH2O	-
6	PROPEOOH + hv → CH3CHO + CH2O + HO2 + OH	-
7	PROPAOOH + hv → CH2O + CH3CO3 + OH	-
8	MACROOH + hv → 2.0OH + 1.68CO + 0.32CH2O + 2.0HO2	-
9	MEKOOH + hv → 2.0OH + 1.86CH3CHO + 1.2CH3CO3 + 0.14CH2O	-
10	ALKENOOH + hv → 2.0OH + 2.0HO2 + 0.33CH2O + 1.36CH3CHO	-
11	ALKANOOH + hv → 0.716CH3COCH3 + 1.028MEK + 0.012CH2O + 0.908CH3CHO	-
12	GLYALD + hv → CO + 2.0HO2 + CH2O	-
13	HYAC + hv → CH3CO3 + HO2 + CH2O	-
14	ISOPOOH+ hv → 0.402MVK + 0.288MACR + 0.69CH2O + HO2	-
15	DMS + OH + M + O2→ 0.6SO2 + 0.4DMSO + 1.2CH2O + 0.007COS	2.00e-12
16	C2H4 + OH + M → 0.75EO2 + 0.5CH2O + 0.25HO2 + M	k_0=1.1e-28e(T/298)$^{-3.5}$; k_∞=8.5e-12e(T/298)$^{-1.75}$; F_c=1.15
17	MPAN + OH + M→ 0.5HYAC + 0.5NO3 + 0.5CH2O + 0.5HO2	9.6e-12exp(-360/T)
18	CH4 + O1D → H2 + CH2O	8.75e-12
19	CH3O + O2 → CH2O + HO2	3.9e-14exp(-900/T)
20	CH3O + NO2 → HNO2 + CH2O	1.1e-11exp(-1200/T)
21	CH3OH + OH → CH2O + HO2 + H2O	2.90e-12exp(-345/T)
22	CH3O2 + CH3O2 → CH3OH + CH2O + O2	9.5e-14exp(390/T)
23	CH3O2 + OH → 0.1CH3OH + 0.9CH2O + 2HO2	3.7e-11exp(350/T)
24	CH3OOH + OH → CH2O + OH + H2O	1.14e-12exp(200/T)
25	CH2O + OH → HCO + H2O	5.5e-12exp(125/T)
26	CH2O + O → OH + HCO	3.4e-11exp(-1600/T)
27	CH2O + NO3 → HCO + HNO3	5.80e-16
28	CH3 + O → CH2O + H	1.10e-10
29	CH3 + O3 → CH2O + HO2	5.4e-12exp(-220/T)
30	Cl + CH2O → HCO + HCl	8.1e-11exp(-30/T)
31	CH2O + Br → HCO + HBr	1.7e-11exp(-800/T)
32	C2H5O2 + CH3O2 → 0.74CH2O + 0.74CH3CHO + 0.96HO2 + 0.26CH3OH + 0.26C2H5OH	2.00e-13
33	C3H7O2 + CH3O2 → 0.695CH2O + 0.78HO2 + 0.128CH3COCH3 + 0.305CH3OH + 0.567CH3CHO	5.18e-12
34	PROPAO2 + NO → NO2 + CH2O + CH3CO3	2.7e-12exp(360/T)
35	PROPAO2 + NO3 → NO2 + CH2O + CH3CO3	2.40e-12
36	PROPAO2 + CH3O2 → 0.3CH3CO3 + 0.8CH2O + 0.5CH3OH + 0.5CH3COCHO + 0.2HYAC + 0.3HO2	7.1e-13exp(500/T)

* MACR (CH2CCH3CHO); MCO3 (CH2CCH3CO3); GLYOXAL (CHOCHO); ONITR (C5H8ONO2); PROPEOOH (C3H6OHOOH); PROPAOOH (CH3COCH2OOH); MACROOH (C4H8O4); MEKOOH (C4H8OO2); ALKENOOH (C4- and higher alkenyl hydroperoxides); ALKANOOH (C4- and higher alkanyl hydroperoxides); MEK (CH3CH2COCH3); GLYALD (HOCH2CHO); HYAC (CH3COCH2OH); ISOPOOH (HOCH2COOHCH3CHCH2); MVK (CH2CHCOCH3); DMS (CH3SCH3); DMSO (CH3SOCH3); EO2 (HOCH2CH2O2); MPAN (CH2CCH3CO3NO2); PROPAO2 (CH3COCH2O2).

Table S2. (continued).

N	HCHO-related reactions	Rate coefficient
37	C2H4 + O3 → 1.0CH2O + 0.46CO + 0.16HO2 + 0.08OH + 0.17CO2 + 0.37O3OLSB	1.2e-14exp(-2630/T)
38	C3H6 + O3 → 0.6324CH2O + 0.341CH3O2 + 0.0868CH4 + 0.4166CO + 0.0124CH3OH + 0.2096HO2 + 0.2474OH + 0.38CH3CHO + 0.2754CO2 + 0.308O3OLSB	6.51e-15exp(-1900/T)
39	PROPEO2 + NO → CH3CHO + CH2O + HO2 + NO2	2.7e-12exp(360/T)
40	PROPEO2 + NO3 → CH3CHO + CH2O + HO2 + NO2	2.40e-12
41	PROPEO2 + CH3O2 → 0.305CH3OH + 0.78HO2 + 1.085CH2O + 0.032CH3COCHO + 0.39CH3CHO + 0.273CH3COCH3	7.583e-13
42	CH3CO3 + CH3O2 → 0.86CH3O2 + 0.86CH2O + 0.86HO2 + 0.86CO2 + 0.14CH3COOH + 0.14CH2O + 1.0O2	1.3e-12exp(640/T)
43	ISOP + O3 → 0.42CH2O + 0.27CO + 0.09HO2 + 0.44O3OLSB + 0.42MACR + 0.16MVK + 0.18OH + 0.05C3H6 + 0.07H2 + 0.15CO2	11.01e-15exp(-2000/T)
44	ISOPO2 + NO → 0.51CH2O + 0.23MACR + 0.37HYDRALD + 0.08ONITR + 0.92NO2 + 1.0HO2 + 0.32MVK	4.4e-12exp(180/T)
45	ISOPO2 + NO3 →1.0HO2+ 0.6CH2O + 1.0NO2 + 0.25MACR + 0.35MVK + 0.4HYDRALD	2.40e-12
46	ISOPO2 + CH3O2 → 0.25CH3OH + 1.0HO2 + 1.2CH2O + 0.19MACR + 0.26MVK + 0.3HYDRALD	5.0e-12exp(400/T)
47	ISOPO2 + CH3CO3 → 1.0CH3O2 + 1.0HO2 + 0.6CH2O + 0.25MACR + 0.35MVK + 0.4HYDRALD	1.40e-11
48	ISOPNO3 + NO → 1.206NO2 + 0.794HO2 + 0.072CH2O + 0.167MACR + 0.039MVK + 0.794ONITR	2.7e-12exp(360/T)
49	ISOPNO3 + NO3 → 1.206NO2 + 0.794HO2 + 0.072CH2O + 0.167MACR + 0.039MVK + 0.794ONITR	2.40e-12
50	ISOPNO3 + HO2 → 1.0XOOH + 0.206NO2 + 0.794HO2 + 0.008CH2O + 0.167MACR + 0.039MVK + 0.794ONITR	1.9e-13exp(1300/T)
51	ISOPNO3 + CH3O2 → 0.06NO2 + 0.711HO2 + 0.697CH2O + 0.059MACR + 0.001MVK + 0.635ONITR + 0.305CH3OH	1.7491e-12
52	APINO2 + CH3O2 → 0.305CH3OH + 1.085CH2O + 0.39PCHO + 0.39HO2	1.22e-13
53	APINO3 + CH3O2 → 0.335CH2O + 1.0CO2 + 0.665CH2O + 0.665HO2 + 0.665CH3COCH3 + 1.33PROPEO2	4.52e-12
54	MCO3 + NO → NO2 + CH2O + CH3CO3	5.3e-12exp(360/T)
55	MCO3 + NO3 → NO2 + CH2O + CH3CO3	5.00e-12
56	MCO3 + CH3O2 → 1.665CH2O + 0.665HO2 + 0.665CH3CO3 + 0.665CO2	4.52e-12
57	MCO3 + CH3CO3 → 2.0CO2 + 1.0CH3O2 + 1.0CH2O + 1.0CH3CO3	4.6e-12exp(530/T)
58	MCO3 + MCO3 → 2.0CO2 + 2.0CH2O + 2.0CH3CO3	2.3e-12exp(530/T)
59	PCO3 + CH3O2 → CH2O + 0.665HO2 + 0.665XO2 + 0.665PROPEO2	4.52e-12
60	MACR + O3 → 0.34CH2O + 0.2OH + 0.14CO2 + 0.35O3OLSB + 0.8CH3COCHO + 0.13HO2 + 0.37CO + 0.1H2	1.5e-15exp(-2110/T)
61	MVK + O3 → 0.05CH2O + 0.95CH3COCHO + 0.08OH + 0.15HO2 + 0.44CO + 0.16CO2 + 0.35O3OLSB + 0.12H2	7.5099e-16exp(-1521/T)

* PROPEO2 (C3H6OHO2); ISOP (C5H8); O3OLSB (secondary and generic species produced during the oxydation of alcenes); ISOPO2 (C5H8OHO2); MACR (CH2CCH3CHO); HYDRALD (HOCH2CCH3OOCH3CHCHO); ISOPNO3 (nitrate radical adduction to isoprene); XOOH (counter for organic hydroperoxides); APINO2 (peroxy radicals from APIN); PCHO (C10H16); APINO3 (ozone adduction to terpenes); MCO3 (CH2CCH3CO3); PCO3 (carboxy radicals from APIN); XO2 (counter for organic peroxy radicals); PROPEO2 (C3H6OHO2); MVK (CH2CHCOCH3).

Table S2. (continued).

N	HCHO-related reactions	Rate coefficient
62	MACRO2 + NO → 0.25CH3COCHO + 0.22HYAC + 0.53CH3CO3 + 0.25CH2O + 0.53GLYALD + 0.22CO + 0.47HO2 + 1.0NO2	2.7e-12exp(360/T)
63	MACRO2 + NO3 → 0.25CH3COCHO + 0.22HYAC + 0.53CH3CO3 + 0.25CH2O + 0.53GLYALD + 0.22CO + 0.47HO2 + 1.0NO2	2.40e-12
64	MACRO2 + CH3O2 → 0.24CH3COCHO + 0.23HYAC + 0.26CH3CO3 + 0.88CH2O + 0.26GLYALD + 0.11CO + 0.73HO2 + 0.25CH3OH	5.0e-13exp(400/T)
65	MACRO2 + CH3CO3 → 0.25CH3COCHO + 0.22HYAC + 0.53CH3CO3 + 0.25CH2O + 0.53GLYALD + 0.22CO + 0.74HO2 + 1.0CH3O2	1.40e-11
66	ONITUO2 + NO → 0.116CH2O + 0.386CH3CHO + 0.209MEK + 1.294NO2 + 0.4HO2 + 0.395XO2 + 0.706ONITR	2.7e-12exp(360/T)
67	ONITUO2 + NO3 → 0.116CH2O + 0.386CH3CHO + 0.209MEK + 1.294NO2 + 0.4HO2 + 0.395XO2 + 0.706ONITR	2.40e-12
68	MEKO2 + NO → 1.0NO2 + 1.329CH3CHO + 0.6CH3CO3 + 0.07CH2O + 0.4HO2 + 0.197MEK	2.7e-12exp(360/T)
69	MEKO2 + NO3 → 1.0NO2 + 1.329CH3CHO + 0.6CH3CO3 + 0.07CH2O + 0.4HO2 + 0.197MEK	2.40e-12
70	MEKO2 + CH3O2 → 0.305CH3OH + 0.699HO2 + 0.75CH2O + 0.086CH3CO3 + 0.295MEK + 0.042CH3COCHO + 0.645CH3CHO	9.76e-13
71	ALKANO2 + NO3 → 0.517MEK + 0.001CH2O + 0.454CH3CHO + 1.0NO2 + 0.562HO2 + 0.336XO2 + 0.101CH3O2	2.40e-12
72	ALKANO2 + CH3O2 → 0.305CH3OH + 0.626HO2 + 0.696CH2O + 0.315MEK + 0.14XO2 + 0.012CH3O2 + 0.045CH3COCH3 + 0.442CH3CHO	3.76524e-13
73	AROMO2 + CH3O2 → 0.305CH3OH + 0.915HO2 + 0.695CH2O + 0087CH3COCHO + 0.135CO + 0.135CH3CO3	2.31e-13
74	HOCH2OO → CH2O + HO2	2.40e+12exp(-7000/T)
75	CH2O + HO2 → HOCH2OO	9.70e-15exp(625/T)
76	EO → 2CH2O + HO2	1.60e+11exp(-4150/T)
77	GLYALD + OH → 0.8CO2 + HO2 + 0.2GLYOXAL + 0.8CH2O	1.00e-11
78	XO2 + CH3O2 → 0.3CH3OH + 0.8HO2 + 0.7CH2O + 0.2CO + 0.1HYAC + 0.1GLYOXAL+ 0.1CH3COCHO + 0.1GLYALD	5.0e-13exp(440/T)
79	DMS + OH → SO2 + 2CH2O + 0.007COS	1.2e-11exp(-280/T)
80	DMS + NO3 → SO2 +NO2 + 2CH2O	1.9e-13exp(530/T)

* MACRO2 (CH3COCHO2CH2OH); HYAC (CH3COCH2OH); ONITUO2 (peroxy radicals from unreactive organic nitrates + OH); MEK (CH3CH2COCH3); MEKO2 (C4H7OO2); ALKENO2 (C4- and higher alkenyl peroxy radicals); ONITU (C3H7ONO2); ALKANO2 (C4- and higher alkanyl peroxy radicals); MEK (CH3CH2COCH3); AROMO2 (peroxy radicals from aromatic compounds); EO (HOCH2CH2O); GLYALD (HOCH2CHO); GLYOXAL (CHOCHO); XO2 (counter for organic peroxy radicals); DMS (CH3SCH3); DMSO (CH3SOCH3); ASMSAM (CH3SO3H).

Table S3. Correlation coefficient of monthly isoprene emissions and meteorological factors and LAI. Regional classification is seen in Fig. S6.

Correlation coefficient (R)	**Temperature**	**LAI**	**Radiation**	**SPEI**
AMZ (Amazon)	0.76	-	0.82	-0.48
EQAF (Equatorial Africa)	-	0.72	-	-
RSAM (Rest of Southern America)	0.75	0.41	0.82	-0.25
NAF (Northern Africa)	0.92	0.88	0.69	0.26
SEAS (Southeast Asia)	0.79	0.73	-	-0.23
CHN+KAJ (China+Korea+Japan)	0.91	0.98	0.71	0.24
SAS (South Asia)	0.79	0.72	-	-
SAF (Southern Africa)	0.92	0.52	0.87	-
MIDE (Mideast)	0.95	0.74	0.80	-
USA (the United States)	0.96	0.98	0.85	-
RUS+CAS (Russia+Central Asia)	0.93	0.98	0.82	-0.56
OCE (Oceania)	0.91	0.40	0.94	-
CAM (Central America)	0.93	0.84	0.65	-
EU (Europe)	0.96	0.97	0.90	-0.31
CAN (Canada)	0.90	0.98	0.70	
Global total	0.92	0.89	0.62	-0.43

*Insignificant correlations ($p>0.05$) are labeled with "-" in the table.

Table S4. Regional and global annual isoprene emissions from 2013 to 2020 (TgC yr^{-1}). Regional classification is seen in Fig. S6.

Isoprene (TgC yr^{-1})	**2013**	**2014**	**2015**	**2016**	**2017**	**2018**	**2019**	**2020**
AMZ	67	71	75	72	69	67	72	74
EQAF	52	51	51	53	50	53	55	55
RSAM	43	45	47	46	41	44	48	45
NAF	39	39	39	39	37	40	43	42
SEAS	34	36	34	36	35	36	38	37
CHN+KAJ	35	32	32	35	33	35	35	35
SAS	32	28	28	30	31	28	34	35
SAF	25	26	25	26	23	28	28	27
MIDE	22	23	23	23	21	23	25	24
USA	25	24	26	26	23	26	27	24
RUS+CAS	19	18	19	20	19	19	21	21
OCE	22	21	21	20	21	22	22	19
CAM	14	13	15	14	13	14	16	14
EU	11	11	11	11	11	12	12	11
CAN	8	9	8	8	7	9	8	8
Global	447	447	453	459	435	456	485	471

Table S5. Regional and global annual mean isoprene emission rates from 2013 to 2020 (unit: 10^{-10} kgC m^{-2} s^{-1}). Regional classification is seen in Fig. S6.

Isoprene (10^{-10} kgC m^{-2} s^{-1})	**2013**	**2014**	**2015**	**2016**	**2017**	**2018**	**2019**	**2020**
AMZ	2.9	3.1	3.3	3.1	3.0	2.9	3.1	3.2
SEAS	2.2	2.3	2.2	2.3	2.3	2.3	2.5	2.4
SAS	2.0	1.7	1.8	1.8	1.9	1.8	2.1	2.1
EQAF	2.0	1.9	1.9	2.0	1.9	2.0	2.1	2.1
CAM	1.6	1.6	1.8	1.7	1.6	1.7	1.9	1.7
RSAM	1.3	1.4	1.4	1.4	1.2	1.3	1.5	1.4
SAF	1.2	1.3	1.2	1.2	1.1	1.3	1.4	1.3
MIDE	1.1	1.2	1.2	1.2	1.1	1.2	1.3	1.2
CHN+KAJ	1.1	1.0	1.0	1.1	1.0	1.1	1.1	1.1
USA	1.0	1.0	1.1	1.1	0.9	1.1	1.1	1.0
NAF	0.8	0.8	0.8	0.8	0.8	0.8	0.9	0.9
OCE	0.9	0.8	0.8	0.8	0.8	0.9	0.9	0.8
EU	0.6	0.6	0.6	0.6	0.6	0.7	0.7	0.6
RUS+CAS	0.3	0.3	0.3	0.3	0.3	0.3	0.3	0.3
CAN	0.2	0.2	0.2	0.2	0.2	0.2	0.2	0.2
Global	1.1	1.1	1.1	1.1	1.0	1.1	1.2	1.1

References

Burkholder, J. B., Sander, S. P., Abbatt, J., Barker, J. R., Cappa, C., Crounse, J. D., Dibble, T. S., Huie, R. E., Kolb, C. E., Kurylo, M. J., Orkin, V. L., Percival, C. J., Wilmouth, D. M., and Wine, P. H.: Chemical Kinetics and Photochemical Data for Use in Atmospheric Studies, Evaluation No. 19, JPL Publication 19-5, Jet Propulsion Laboratory, http://jpldataeval.jpl.nasa.gov, 2019.

Guy, B. and Susan, S.: Aeronomy of the Middle Atmosphere: Chemistry and Physics of the Stratosphere and Mesosphere, Atmospheric Science Library, D. Reidel Pub. Co., 2nd edn., 1987.

Li, W., MacBean, N., Ciais, P., Defourny, P., Lamarche, C., Bontemps, S., Houghton, R. A., and Peng, S.: Gross and net land cover changes in the main plant functional types derived from the annual ESA CCI land cover maps (1992–2015), Earth Syst. Sci. Data, 10, 219-234, 10.5194/essd-10-219-2018, 2018.

Madronich, S. and Flocke, S.: The Role of Solar Radiation in Atmospheric Chemistry, in: Environmental Photochemistry, edited by: Boule, P., Springer Berlin Heidelberg, Berlin, Heidelberg, 1-26, 10.1007/978-3-540-69044-3_1, 1999.

Pu, J., Yan, K., Roy, S., Zhu, Z., Rautiainen, M., Knyazikhin, Y., and Myneni, R. B.: Sensor-independent LAI/FPAR CDR: reconstructing a global sensor-independent climate data record of MODIS and VIIRS LAI/FPAR from 2000 to 2022, Earth Syst. Sci. Data, 16, 15-34, 10.5194/essd-16-15-2024, 2024.